5-2014

THE EPIGENETICS OF SMALL CELL PROSTATE CANCER

Brittany N. Kleb

THE EPIGENETICS OF SMALL CELL PROSTATE CANCER

by

Brittany North Kleb, BS

APPROVED:

Ana Aparicio, MD
Supervisory Professor

Jill Schumacher, PhD

Marcos Estecio, PhD

Sean Post, PhD

Elsa Flores, PhD

APPROVED:

Dean, The University of Texas
Graduate School of Biomedical Science

THE EPIGENETICS OF SMALL CELL PROSTATE CANCER

A

THESIS

Presented to the Faculty of The University of Texas Health Science Center at Houston and The University of Texas MD Anderson Cancer Center Graduate School of Biomedical Sciences in Partial Fulfillment

of the Requirements

for the Degree of

MASTER OF SCIENCE

by

Brittany North Kleb, BS

Houston, Texas

May, 2014

DEDICATION

I dedicate this thesis to my two amazing sons, Cameron and Caden, may the advances in science pave the way for a promising future full of opportunities. Also, to my husband, Brian, for his unconditional love and support.

ACKNOWLEDGEMENTS

It is with great appreciation that I acknowledge and thank Dr. Ana Aparicio for her patience, guidance, and encouragement. Her zealous attitude toward scientific research and compassion for her patients fuels my passion for science. She constantly challenges my scientific knowledge and it has been a true pleasure to train with her.

I would like to also thank the members of my advisory and supervisory committees, Dr. Marcos Estecio, Dr. Sean Post, Dr. Jill Schumacher, and Dr. Elsa Flores for their guidance and criticisms, which allowed me to become a better scientist.

Additionally, I would like to thank the members of the Genitourinary Medical Oncology Research team, specifically, Tatianna Robles and Katja Karjalainen for their support and guidance throughout my training.

THE EPIGENETICS OF SMALL CELL PROSTATE CANCER

Brittany North Kleb, BS

Supervisory Professor: Ana Aparicio, MD

Small cell prostate cancer (SCPC) is an androgen receptor (AR) negative variant that can develop during the progression of castration-resistant AR-positive (AR^+) prostate adenocarcinomas. While rare at initial diagnosis, SCPC is present in 10-20% of patients resulting in an aggressive clinical course with poor response to hormonal therapies and a short median survival. Our studies in patient-tumor derived xenografts revealed that the AR-negative small cell prostate carcinomas (AR^-SCPC) express genes involved in neural development instead of the prostate luminal epithelial gene expression that characterizes AR-positive castration-resistant adenocarcinomas (AR^+ADENO). We hypothesized that the differences in cellular lineage programs should be reflected in distinct epigenetic profiles and that they could be reversed with epigenetic drugs. Using Methylated CpG Amplification coupled to Microarray (MCAM) we identified distinctly hypermethylated DNA sequences present in AR^-SCPC but not in AR^+ADENO xenografts. Because MCAM is enriched for CpG islands located around gene transcription start sites and it has been proposed that greater differences occur at CpG shores, we used the Illumina 450K platform to examine additional regions of the genome and we also demonstrated a strong correlation

between the xenografts' DNA methylation profiles and the patient tumors from which they were derived.

Interestingly, we observed a low frequency of AR promoter methylation found in samples that lacked AR expression despite previous publications. Array CGH analysis did not reveal copy number alterations and sequencing by others did not show mutations of the AR gene that could explain its silencing. We found that the AR promoter is enriched in silencing histone modifications (H3K27me3 and H3K9me2) and that EZH2 inhibition with DZNep results in AR re-expression and growth inhibition in AR^-SCPC cell lines. These data support the hypothesis that AR^-SCPC are epigenetically distinct from AR^+ADENO tumors and that epigenetic therapies may reverse the AR^-SCPC phenotype.

Keywords: castrate-resistant prostate cancer, small cell prostate cancer, DNA methylation profiling, methylome, histone modifications, EZH2, androgen receptor, epigenetics, PRC2, DZNep

TABLE OF CONTENTS

LIST OF ILLUSTRATIONS

LIST OF TABLES

Introduction

Prostate Cancer

Prostate cancer (PCa) is the most common malignancy in males with an estimated 233,000 new cases diagnosed in 2014 the United States with 29,480 deaths due to the disease [American Cancer Society, 2014]. Prostate tumors are clinically heterogeneous, where some patients die of metastatic disease within 2–3 years of diagnosis while others can live for 10–20 years with organ-confined disease [1]. The wide range of survival outcomes is observed due to the underlying biological heterogeneity of the disease. A better understanding of the drivers of disease progression in each subset will lead to implementation of specific therapies for each subset improving overall patient survival. Castration remains the most effective way to control the disease and continues to be the first line of treatment, however, the majority of deaths are due to resistance to this therapy regimen. Currently the clinical model of prostate cancer progression is defined by pathological classifications where morphological features of the tumor determine a Gleason sum score [2]. These resulting scores group patients into clinical stages and ultimately determine treatment plans. A Gleason score is also an important prognostic determinate where high scores predict more rapid progression and aggressive treatments [3]. While Gleason scores and staging are important in early treatment decisions, as the disease progresses the clinical management of CRPC is limited. All CRPCs are treated the same even though the tumors behave very different. Molecular classification and resulting molecular

markers of progression are necessary for proper diagnosis and treatment of this disease.

AR Centered Disease

The androgen receptor is a ligand dependent transcription factor. It resides in the cytoplasm as a protein complex composed of heat shock proteins in a ligand free, inactive state. Activation of the AR is dependent on androgen signaling. Circulating testosterone enters the prostate cell, where it is converted to dihydrotestosterone (DHT) by the enzyme 5a-reductase. Activation of the androgen receptor occurs through the binding of DHT resulting in a conformational change. This leads to dissociation from the heat shock proteins, receptor phosphorylation and the formation of a homodimer complex. This homodimer complex then travels to the nucleus where is can bind to androgen response elements on target genes to recruit co-regulatory proteins, co-activators or co-repressors triggering transcriptional activation or repression of various genes. Its ability to regulate genes that both stimulate proliferation and inhibit apoptosis through androgen stimulation makes AR important in the growth and survival of prostate cancer cells.

Therefore, prostate cancer depends on a crucial level of androgenic stimulation and androgen ablation is the primary therapy for prostate cancer. Prostate cancer can progress following castration (CRPC) and most remain sensitive to secondary hormone therapies due to the activity of the androgen receptor [4, 5]. However, approximately 20% of men who die of CRPC have

tumors with small cell carcinoma morphology, a variant that loses AR expression, is resistant to hormonal therapies [6], and predicts for a poor clinical outcome [7, 8].

Molecular Classification of Prostate Cancer

The molecular mechanisms of prostate cancer progression have been centered on the androgen receptor, the tumor microenvironment, oncogenes and tumor suppressors. Loss of tumor suppressor genes PTEN, p53, and RB is critical and common in prostate cancer progression. The loss of PTEN results in the upregulation of the PI3K pathway and frequently observed in metastatic disease. Its loss is also linked to shorter progression-free and overall survival but not a predictive measure of response to specific therapies [9, 10]. The tumor suppressor RB is known to protect against tumor development through the suppression of cell cycle progression genes. The loss of RB is linked to more advanced stages of CRPC, and could be used as a predictive marker of response to therapies [11]. However, the role of RB in castration resistant disease transition from AR positive to small cell phenotype is not well established, although their response to chemotherapy could be due to RB loss.

Aberrant activation of oncogenes is prevalent in the late stage of prostate cancer progression, including Src, MET, Axl, and FGFR. The most frequent oncogenic event in prostate cancer is the TMPRSS2:ERG gene fusion resulting in overexpression of the ERG gene, a transcription factor that regulates cellular proliferation and PI3K pathway activation [12, 13]. Additionally this gene fusion

does not correlate with adverse tumor characteristics or poor prognosis. [14] In fact TMPRESS2:ERG is associated with low grade disease [15]. AR negatively regulates the oncogene c-Met and therefore with androgen ablation, overtime the MET receptor is overexpressed triggering tumor growth and blood vessel formation [16]. The non-receptor tyrosine kinase, c-Src, regulates a complex signaling network that drives the development of castrate resistance through multiple biological processes. Inhibitors of this pathway have been used in clinical trials and shown efficacious in limited subset of tumors. The activation of oncogenic pathways also affects AR function through AR phosphorylation or direct association of the receptor [17, 18].

SCPC

Along with small cell morphological features, SCPC also displays distinct clinical characteristics including frequent visceral metastases, lytic bone involvement, relatively low PSA, resistance to androgen ablation therapy, and high response rates to chemotherapy [8]. SCPC is a rare finding at the time of initial prostate cancer diagnosis and most frequently found during the castration resistant progression of the disease mixed with adenocarcinoma components [19]. This unique clinical phenotype can be observed in the absence of small cell carcinoma morphology but that it maintains its specific molecular profile: loss of tumor suppressors (pRb, p53), switch from epithelial to neural progenitor/stem cell program and aberrant mitotic gene expression [3, 20, 21]. There is a marked increase in mitotic genes, especially M-phase transition genes, including AURKA,

PLK1 and UBE2C [22]. Histopathological evaluation of these mixed tumor specimens display what appears to be a gradual transition from the adenocarcinoma to the SCPC component [11]. In addition, several groups have shown concordance in the *ERG* rearrangements present in the morphologically distinct components of the same tumor [9, 23] suggesting that both arise from a common cell of origin. SCPCs lose features of the luminal prostate epithelium and adopt a neural precursor phenotype with increased levels of pro-neural transcription factor expression including *ASCL1* and *MYCN* [20, 21, 24-27]. *MYCN* is highly expressed in early embryogenesis and in cancers that originate from embryonic or neuroendocrine tissues such as small cell lung cancer [27], suggesting SCPCs have a neural developmental program [28]. Therefore, the molecular switch from epithelial to neural/progenitor stem cell program occurs through a transdifferentiational switch, implicating an underlying epigenetic mechanism might exist.

Prostate Cancer Epigenetics

Epigenetics refers to functionally relevant genomic information not coded by the DNA sequence and heritable during cellular division. There are multiple epigenetic modifications that contribute to the initiation and progression of prostate cancer including DNA methylation, histone modifications, microRNAs, long noncoding RNAs, and post translational modifications.

DNA Methylation

Methylation of DNA cytosine residues that precede guanine (CpG) is tightly associated with gene regulation and occurs in short stretches of CpG-rich regions found in the promoters of about 60% of genes [29]. These CpG rich regions are known as CpG islands (CGIs) and are generally unmethylated in normal cells. However, in cancer cells, aberrant hypermethylation, a gain of methylation, occurs in promoter CGIs resulting in gene silencing and loss of function [30]. Conversely, global hypomethylation is commonly observed in tumors resulting in genomic instability through the resultant change in chromatin structure. DNA methylation profiling of CRPC could expose key subset of genes modified and used as markers or reveal an underlying biological mechanism of the disease. A list of promoter methylation at the single gene level has been reported in prostate cancer, including GSTPI, AR, APC, RASSF1, and CDH1 with functional consequences. There are very few studies investigating the epigenomic landscape of CRPC. In 2004, Yegnasubramanian et al. reported on the methylation of 16 promoter CpG islands in 83 metastatic samples obtained at autopsy from 28 men who had been treated with androgen-deprivation therapy [31]. Those investigators also observed that CRPC metastatic sites had significantly lower levels of 5-methylcytosine and of long interspersed elements 1 (LINE1) methylation, a marker of global methylation, than did the primary and untreated prostate cancer tissues, and they found decreased methylation in the promoter CGIs of a group of cancer–testis genes in metastatic tissues [31, 32]. In subsequent studies, a very similar methylation pattern in primary and

metastatic prostate cancer tissues that was maintained across metastatic sites within a patient, but methylation patterns in different patients appeared heterogeneous [33]. However, those findings did not appear to hold true in the AR^{-} prostate cancer cell lines PC-3 and DU145, and again, the between-patient heterogeneity appeared greater than that within given patients. Another study profiled the DNA methylome of 15 liver and soft tissue metastatic CRPC samples obtained at autopsy and observed three of their 15 samples with a hypomethylated phenotype relative to that of the rest [34]. Of these previous studies, the investigators were unable to show significant correlation with clinicopathologic or molecular features within the samples [33, 34].

Therefore, we hypothesized DNA methylation could thus be used to classify CRPC into clinically relevant predictive subgroups, performing genome-wide DNA methylation profiling of 34 human prostate cancer xenografts obtained from 24 castrate patients, using methylated CpG amplification coupled to microarray (MCAM) analysis. We identified distinctly hypermethylated DNA sequences in AR^{-}SCPC versus AR^{+}ADENO xenografts. Because MCAM is enriched for CpG islands located around gene transcription start sites we used the Illumina 450K platform to examine additional regions of the genome and to demonstrate correlation between the xenografts' DNA methylation profiles and the patient tumors from which they were derived. We focused on site-specific DNA methylation at the AR CpG island. There was a low frequency of AR promoter methylation found in samples that lacked AR expression. We continued

our investigation of the AR promoter region by evaluating the histone modification patterns.

Histone Modifications & EZH2

In eukaryotes, DNA is packaged by winding itself around repeating units of nucleosomes composed of histone protein complexes. The nucleosome is comprised of 147 base pairs of DNA wrapped around an octamer of histones (2 each of H2A, H2B, H3, and H4). Nucleosomes are then coiled into higher order structures to allow for chromatin compaction and are essential for gene regulation. The local structure of the chromatin influences DNA accessibility and determines distinct patterns of gene expression. Open chromatin allows for the recognition of specific DNA sequences by transcription factors, enhancers, and polymerases essential for gene transcription whereas closed chromatin restricts access to the DNA. There are two mechanisms that control the accessibility of chromatin and subsequent gene transcription—displacement of histones by chromatin remodeling complexes and enzymatic modifications to histones. Post-translational modifications to the histones include the addition or removal of acetyl, methyl, phosphate, or ubiquitin groups to the amino-terminal tails histone tails. Each modification affects the chromatin in different ways by either recruiting regulatory proteins or altering the structural components of the chromatin. Lysine methylation is predominately used to regulate chromatin structure with the addition of three methyl groups on H3 lysine 4 (H3K4me3) resulting in open

chromatin and active gene expression and the contrasting tri-methylation of H3 lysine 27 (H3K27me3) produces closed chromatin and gene suppression.

A class of proteins that control the chromatin organization are the Polycomb group (PcG) proteins. They function as key epigenetic regulators of gene transcription through multimertic complexes catalyzing the covalent additions to the histone tails and writing the histone code. These proteins were originally discovered as repressors of a family of developmental genes, the homeodomain-containing transcription factors (Hox) in *Drosophila melanogaster* and essential in normal mammalian development [35]. They comprise two distinct Polycomb repressive complexes (PRC1 and PRC2) functioning together to maintain long term silencing [35]. One such cooperation includes the trimethylation of H3K27 by PRC2 mediates the recruitment of PRC1 to the gene loci to elicit further consolidation of the condensed chromatin. Enhancer of zeste homolog 2 (EZH2) is the protein necessary for the catalytic function of PRC2 complex with its SET domain as the active site for the methylation reaction. In order for EZH2 to function enzymatically, two other proteins must also be involved, embryonic ectoderm development (EED) and suppressor of zeste 12 (SUZ12). These three proteins along with two histone binding proteins retinoblastoma binding protein 4 and 7 (RBBP4 and RBBP7) make up the core components of PRC2 [36]. Overexpression of EZH2 has been shown in multiple solid tumors including breast, bladder, gastric, and prostate cancer [37-40]. It was first associated with prostate cancer in 2002 by a cDNA microarray study demonstrating its upregulation prominently in metastatic prostate cancer as

compared to localized disease [38]. Additionally, the results indicated a positive relationship between EZH2 protein level and disease aggressiveness [38]. Global upregulation of EZH2 could result in increased H3K27me3 at key tumor suppressor gene loci. Therefore we challenged that EZH2 mediated H3K27me3 could play a role in the AR gene silencing of the AR^-SCPC. Using ChIP q-PCR we observed enrichment in H3K27me3 at the AR promoter region in our AR^- samples suggesting a possible mechanism of AR silencing in SCPC.

Noncoding RNAs

Noncoding RNAs (ncRNAs) are endogenously transcribed RNA that do not result in protein translation, but function in an epigenetic fashion to control gene expression and protein function. Several ncRNAs are abbarently expressed in prostate cancer. MicroRNAs (miRNAs) function as translational silencers by binding to the target gene's transcribed mRNA and degrading it. Genomic loss of microRNA-101 leads to the overexpression of EZH2 predominately in more aggressive prostate cancers than in localized disease [41]. Additionally long noncoding RNAs (lncRNAs), ncRNAs >200 nucleotides, have been implicated in epigenetic manipulation of gene expression in prostate cancer with both oncogenic and tumor suppressor effects [42]. Interestingly, the lncRNA *ANRIL* supplies two layers of epigenetic regulation of the tumor suppressor p15 by interacting with SUZ12, recruiting PRC2 to the gene loci and silencing the gene in CRPC [43].

Due to the unique way epigenetic alterations control the transcriptional machinery of a gene without disrupting the DNA sequence, they have the potential to be reversed. Therefore inhibitors have been developed to disrupt epigenetic silencing and used as tools to study the biology of diseases along with pharmacological potential. One such molecule, 3-deazaneplanocin-A (DZNep), was developed as a potent inhibitor of S-adenosyl-Lhomocysteine (SAH)-hydrolase, an EZH2 cofactor, and depletes cellular levels of the PRC2 complex resulting in the inhibition of H3K27me3 [44, 45]. We used DZNep as a tool to manipulate SCPC *in vitro* and reveal a surprising epigenetic feature of the disease.

Results

Xenograft and Donor Patient Features

For the MCAM studies, we analyzed DNA extracted from mouse subcutaneous tissue, cultured PrECs and from 34 human prostate cancer xenograft tissues derived from the tumors of 24 patients. The MDA 79, MDA 117, MDA 118b, MDA 144, MDA 146 and MDA 155 xenograft lines and sublines have been previously described [20, 21]. Of the 34 samples, 14 included 2 to 6 xenograft sublines derived from the same donor tumor (eg, 146.10 to 146.12) and 2 biologic replicates (ie, the same xenograft subline but grown in a different mouse; eg, 144-4R) (Table 1).

Table 1. Xenograft Sample Description.

Patient Donor	Xenograft Line-Subline	DMSO or FF	DNA Quantity (ug)	260/280 Ratio	DNA-EP Smear	Morphology	AR (%cells)	% Mouse DNA Avg	% Mouse DNA SD
31	MDA-31	D	828	1.94		ADCA	85±5	1.11	0.00
40	MDA-40	D	435	1.97		ADCA	0±0	1.19	0.22
43	MDA-43	D	1596	1.98		ADCA	80±0	1.30	0.25
44	MDA-44	D	369	1.88		SCPC	0±0	2.00	1.16
46	MDA-46	D	654	1.89		-	-	0.71	0.26
51	MDA-51	D	229	1.94		ADCA	0±0	6.83	0.46
62	MDA-62	D	570	1.93		Mixed ADCA & SARC	0±0	37.15	14.73
66	MDA-66	D	289	1.94		ADCA	0±0	3.79	3.69
75	MDA-75	D	51	1.96		ADCA	90±0	1.54	0.05
76	MDA-76	D	1250	1.90	Yes	ADCA	86±12	14.47	3.02
79	MDA-79	D	522	1.92	Yes	ADCA	89±6	57.41	51.61
80	MDA-80	D	111	1.94		ADCA	90±4	0.97	0.06
91	MDA-91A	D	450	1.96		SCPC	0±0	1.92	0.67
	MDA-91B	D	704	1.89		SCPC	0±0	1.69	0.00
94	MDA-94	D	277	1.96		ADCA	0±0	3.56	2.81
100	MDA-100	D	190	1.93		SQ CELL CA	0±0	9.32	3.10
101	MDA-101	D	1422	1.94	Yes	ADCA	63±20	7.92	4.11
102	MDA-102	D	909	1.93	Yes	-	-	12.84	6.87
117	MDA-117-9	FF	554	1.90		ADCA	96±2	1.28	0.41
118	MDA-118b	FF	308	1.91		ADCA	0±0	57.38	21.00
122	MDA-122	FF	880	1.97		ADCA	90±0	11.58	2.89
137	MDA-137	FF	763	1.89		ADCA	100±0	10.64	1.69
144	MDA-144-11	FF	540	1.94		SCPC	0±0	5.07	0.28
	MDA-144-13	FF	576	1.95		SCPC	0±0	1.84	0.32
	MDA-144-13R	FF	876	1.89		SCPC	0±0	1.69	0.60
	MDA-144-20	FF	1415	1.98		SCPC	0±0	0.78	0.05
	MDA-144-23	FF	831	1.96		SCPC	0±0	1.24	0.03
	MDA-144-4	FF	1122	1.98		LCNEC	0±0	1.51	0.03
	MDA-144-4R	FF	808	1.92		LCNEC	0±0	1.16	0.78
	MDA-144-6	FF	1398	1.95		LCNEC	1±2	2.53	2.60
146	MDA-146-10	FF	970	1.91		SCPC	0±0	0.66	0.53
	MDA-146-12	FF	1051	2.04		Mixed ADCA & SCPC	97±6	3.35	0.28
155	MDA-155-12	FF	884	1.95		SCPC	0±0	1.01	0.01
	MDA-155-2	FF	1132	1.96		SCPC	0±0	1.35	0.36

Abbreviations: MDA, MD Anderson; DMSO or D, stored in dimethyl sulfoxide; FF, fresh frozen; EP, electrophoresis; ADCA, adenocarcinoma; SCPC, small cell prostate carcinoma; SARC, sarcomatoid; SQ CELL CA, squamous cell carcinoma; LCNEC, large cell neuroendocrine carcinoma; AR, androgen receptor.

Eleven of the 34 samples displayed SCPC morphology, 1 showed mixed ADENO and SCPC features and 3 had large cell neuroendocrine (LCNEC) morphology. LCNEC is a rare variant that bears strong similarities with SCPC and is thought to represent a transitional form between ADENO and SCPC [21]. Additional AR-negative samples included one with squamous cell carcinoma morphology and

another with mixed adenocarcinoma and sarcomatoid features. Paraffin embedded tissues were not available for xenografts MDA 102 and MDA 46, morphology unknown. The remaining 13 samples had ADENO morphology but 5 of these did not express AR by immunohistochemistry. Four DNA samples exhibited a smear on gel electrophoresis, indicating significant DNA degradation; however, a strong high molecular–weight band was still present in all 4. Seven samples had >10% mouse DNA contamination (Table 1; Figure 1). Neither DNA degradation nor mouse DNA contamination affected the quality of the arrays. The

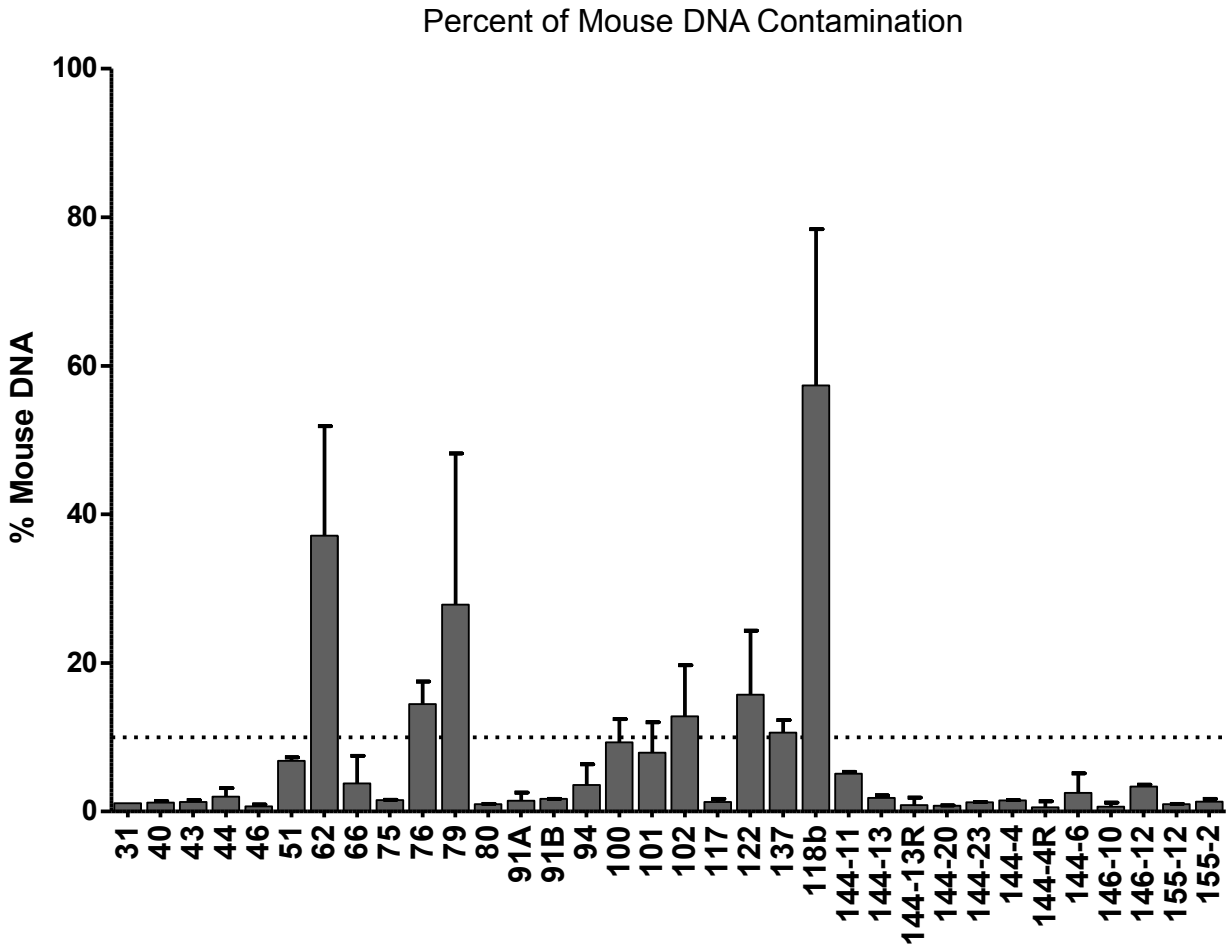

Figure 1. Percent Mouse DNA. The amount of mouse DNA contamination found in xenografts detected by quantitative PCR using the Human and Mouse beta globin gene expression.

charts of the 24 donor patients (4 of whose tumors yielded >1 xenograft line) were retrospectively reviewed (Table 2). All patients had received ADT, and 20 had received at least 1 line of chemotherapy (often containing more than 1 agent) before xenograft establishment. One patient (the donor of MDA-43) remains alive, 16.1 years after diagnosis following bilateral adrenalectomy.

Table 2. Clinical Characteristics of Donor Patients.

Patient Donor	Xenograft Line	Race	Age at Diagnosi	Tumor Site	PSA at Diagnosis ng/mL (n=22)	Metastatic at Diagnosis (n=21)	Metastases to Bone (n=22)	Time on ADT Pre-X (y)	Number of Chemo Regimens Pre-X	Time on Chemo Pre-X (y)	OS from Diagnosis (y)	OS from Start ADT (y)	OS from Start Chemo (y)	OS from Xenograft (y)
31	MDA-31	W	55	Liver	-	No	No	2.4	1	0.7	3.0	2.8	1.1	0.4
40	MDA-40	W	65	Liver	18.5	No	Yes	1.5	2	0.2	4.7	1.7	0.3	0.2
43	MDA-43	B	61	Adrenal	66.7	Yes	No	2.3	0	-	16.4	16.1	-	13.9
44	MDA-44	W	61	SQ nodule	-	Yes	Yes	6.1	2	1.2	6.4	6.4	1.5	0.3
46	MDA-46	W	53	Pleural fluid	32.0	No	Yes	3.0	2	1.8	4.2	3.3	2.1	0.3
51	MDA-51	W	83	Liver	13858.0	Yes	No	2.6	0	-	3.9	3.8	0.7	1.2
62	MDA-62	W	59	Ascitic fluid	5.3	No	No	0.3	3	0.3	1.9	0.4	0.3	0.0
66	MDA-66	W	53	Pelvic tumor	18.4	-	Yes	5.1	2	1.7	8.4	7.3	3.8	2.1
75	MDA-75	B	66	Brain	6.2	No	-	4.4	0	-	5.5	4.5	-	0.1
76	MDA-76	W	64	Pelvic tumor	173.0	No	No	2.6	2	0.9	3.2	2.8	1.2	0.3
79	MDA-79	W	60	Pelvic tumor	65.0	-	Yes	6.2	2	0.9	13.1	11.9	6.6	5.7
80	MDA-80	W	67	Pleural fluid	234.0	Yes	Yes	2.5	3	1.2	3.1	3.1	1.8	0.6
91	MDA-91	W	37	Liver	42.0	Yes	Yes	4.8	3	4.2	6.9	6.8	6.2	2.0
94	MDA-94	W	61	Pleural fluid	4.1	Yes	Yes	3.4	3	2.1	4.2	4.1	2.8	0.7
100	MDA-100	W	69	Pelvic tumor	0.9	No	No	1.0	4	1.0	4.1	4.1	4.1	3.1
101	MDA-101	W	67	Liver	6.4	No	Yes	1.3	2	0.8	3.9	1.7	1.2	0.4
102	MDA-102	W	61	Pelvic tumor	12.3	No	Yes	6.6	1	0.7	14.7	12.0	6.2	5.4
117	MDA-117	H	59	Pelvic tumor	99.2	-	Yes	4.3	1	0.4	5.2	5.2	1.3	0.9
118	MDA-118b	W	47	Bone	5180.0	Yes	Yes	1.6	2	0.4	1.9	1.9	0.7	0.3
122	MDA-122	W	60	Adrenal	7.6	No	-	5.1	0	-	14.4	7.6	-	2.5
137	MDA-137	W	56	RPLN	13.5	No	Yes	6.0	2	0.7	8.0	6.5	1.2	0.6
144	MDA-144	W	67	Pelvic tumor	na	No	No	1.1	2	0.7	4.7	1.4	1.0	0.3
146	MDA-146	W	73	Pelvic tumor	10.7	No	No	1.2	1	0.3	6.1	2.5	1.6	1.3
155	MDA-155	W	72	Pelvic tumor	4.6	Yes	Yes	0.4	2	0.4	0.6	0.6	0.6	0.2

Abbreviations: W, white; B, black; H, hispanic; SQ, subcutaneous; RPLN, retroperitoneal lymph node; PSA, prostate specific antigen; ADT, androgen deprivation therapy; y, years; Chemo, chemotherapy; Pre-X, prior to xenograft development; OS, overall survival.

DNA Methylation Profiles of Patient Tumor Derived Castration Resistant Prostate Cancer Xenografts

Unsupervised hierarchical clustering (Ward linkage, Euclidean distance) using all M values for the 16,621 SmaI sites after LOWESS normalization showed that for the most part, the xenograft lines derived from the same patient clustered together (Figure 2): Only two of the MDA 144 (MDA 144-20 and MDA

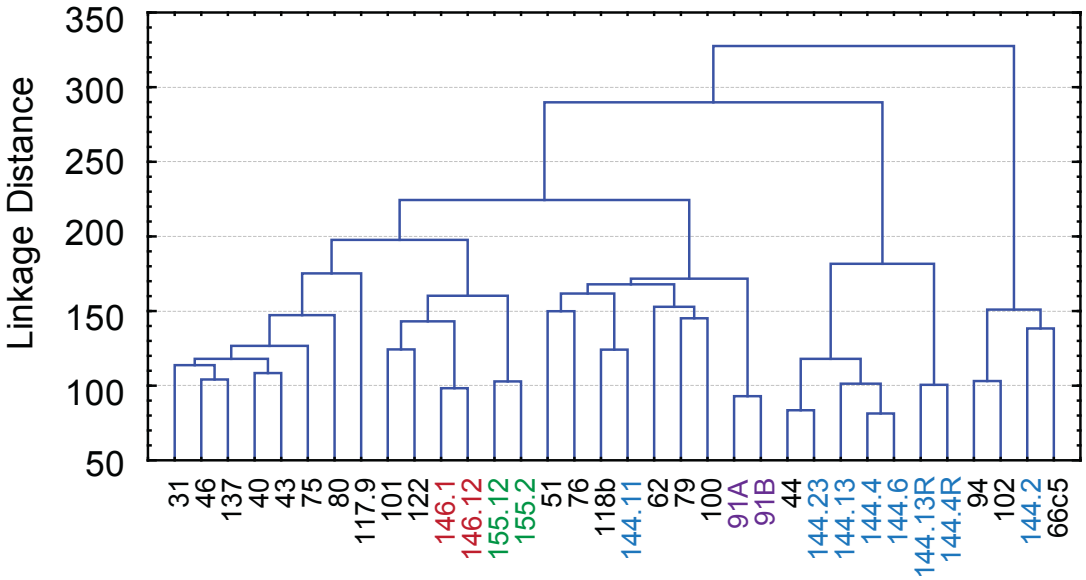

Figure 2. Unsupervised hierarchal clustering. Unsupervised hierarchical clustering (Ward linkage, Euclidean distance) using all M values for the 16,621 SmaI sites after LOWESS normalization

144-11) sublines did not cluster with the other 6 MDA 144 samples. All other xenograft sublines derived from a single patient tumor clustered together (MDA 146-10 with MDA 146-12, MDA 155-12 with MDA 155-2, MDA 91A with MDA 91B). This suggests that the misclassification of the MDA 144-20 and MDA 144-11 sublines might be due to methodological differences and supports the notion that DNA methylomes are stable in xenografts. To validate the MCAM results, we selected 19 sequences contained within 17 promoter-associated (± 1 kb from closest TSS) CGIs for Pyrosequencing. Using 10% as the cutoff for calling a sequence hypermethylated and a normalized log2 ratio of tumor:normal signal ≥1.3, we obtained a sensitivity of 89.8%, a specificity of 67.0%, a positive predictive value of 71.0% and a negative predictive value of 87.9% (Figure 3), consistent with our previous experience with the MCAM method [46].

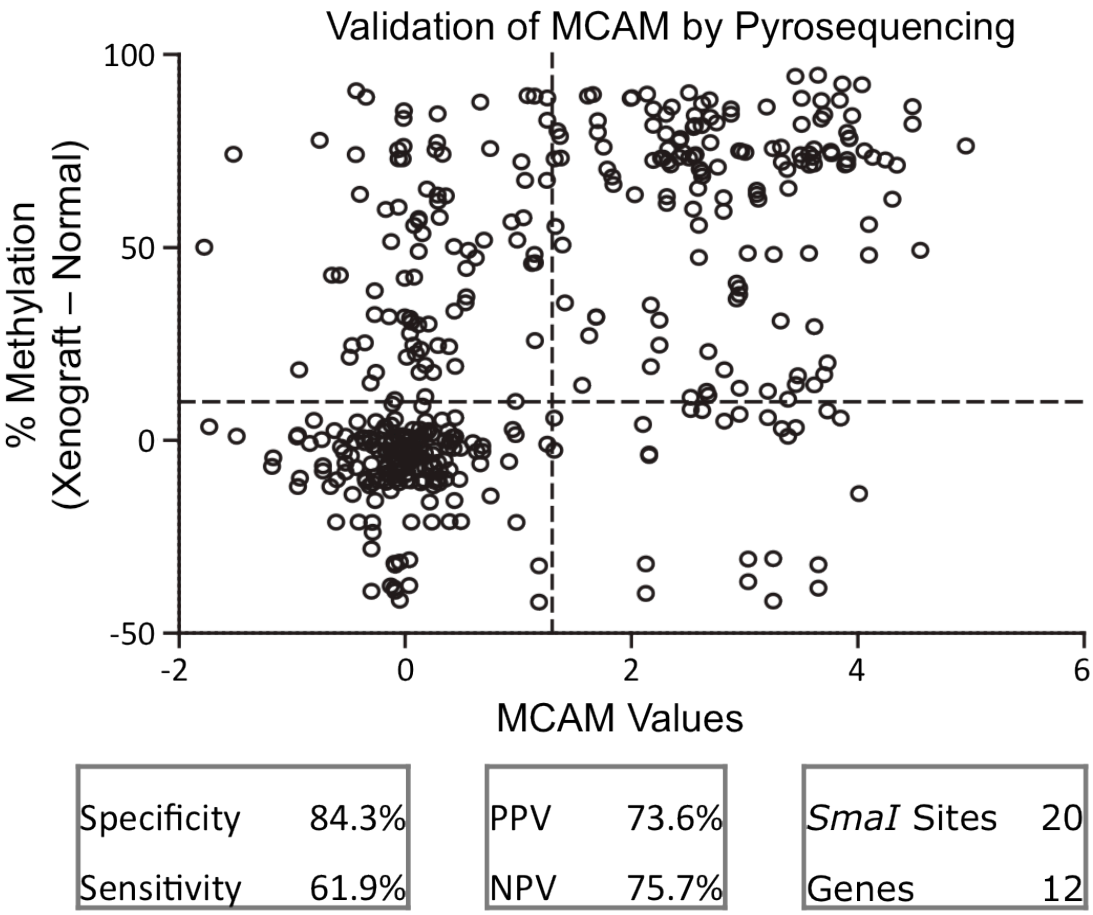

Figure 3. Methylated CpG-island Amplification coupled to CpG island microarray (MCAM) validation. Pyrosequencing was used to measure the % DNA methylation of 19 randomly selected sequences (*Sma I sites*) contained within 17 promoter-associated CpG islands (*Genes*) in the xenograft samples and in the pooled DNA from normal male volunteer peripheral blood mononuclear cells (PBMC). Shown in the y-axis is the % DNA methylation in the xenograft samples minus the % DNA methylation in the pooled normal DNA (*% Methylation Xenograft-Normal*). Shown in the x-axis are the *MCAM M values* (normalized $\log^2$ ratio of xenograft:normal PBMC fluorescent signal). Sequences with M values ≥ 1.3 and % DNA methylation by Pyrosequencing >10% were considered hypermethylated. The number of true negative (n=175), true positive (n=211), false negative (n=86) and false positive (n=34) values are shown in each quadrant and used to calculate the *specificity*, *sensitivity*, positive predictive value (*PPV*) and negative predictive value (*NPV*).

In later analyses, we excluded 1,800 SmaI sites to account for nonspecific hybridization of contaminant mouse DNA in the xenograft DNA samples and for

tissue-specific hypermethylation of prostate cells, compared with normal blood (1,317 from mouse DNA, 553 from PrEC DNA and 70 from both) leaving a total of 14,821 SmaI fragments for analysis. We averaged the log2 ratio values of technical and biologic replicates of the same tumors and, with the 1.3 cutoff, found that the frequency of hypermethylated SmaI fragments ranged from 2.2% to 12.7% (median, 6.6%) per xenograft (Figure 4A). However, 80% of the studied SmaI fragments were unmethylated across all samples, and correlated hypermethylation was rare, with only 527 of 14,821 SmaI fragments (3.5%) being hypermethylated in 50% or more of the tumors.

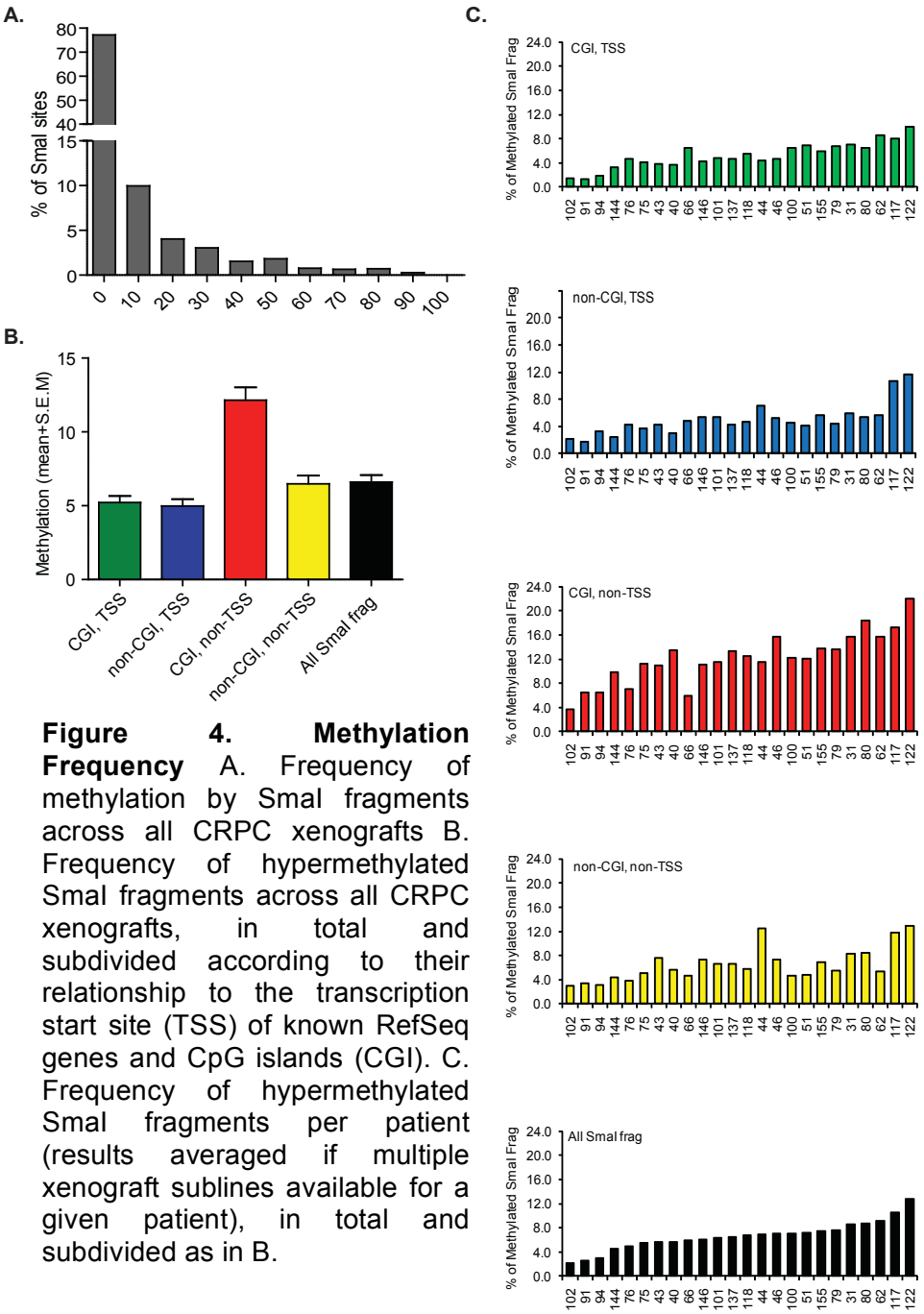

Figure 4. Methylation Frequency A. Frequency of methylation by SmaI fragments across all CRPC xenografts B. Frequency of hypermethylated SmaI fragments across all CRPC xenografts, in total and subdivided according to their relationship to the transcription start site (TSS) of known RefSeq genes and CpG islands (CGI). C. Frequency of hypermethylated SmaI fragments per patient (results averaged if multiple xenograft sublines available for a given patient), in total and subdivided as in B.

We classified the 14,821 SmaI fragments according to their relationship to the promoter region of known RefSeq genes and with CpG islands and examined the frequency of hypermethylation in each compartment. The first clear

observation was that the compartment consisting of nonpromoter CpG islands is generally 2 to 3 times more hypermethylated than any other compartment is and that promoters associated with CpG islands constitute the least-hypermethylated compartment (Figure 4B). Figure 4C is a more detailed presentation of the fractions of hypermethylated SmaI sites in each compartment in the different xenograft lines. In general, there was good agreement: xenograft lines with the lowest frequencies of methylated promoter CpG islands, for example, also had very low frequencies of hypermethylated nonpromoter CpG islands, non-CpG island promoters, and nonpromoter non-CpG island SmaI sites.

DNA methylation markers distinguish AR^+ from AR^- CRPC tumors

To determine whether DNA methylation markers could distinguish the AR^+ from the AR^- xenografts, we used the averaged probe M values per patient converted to categorical values (log2R/G≥1.3 = methylated, log2R/G<1.3 = unmethylated) and focused only on promoter CpG islands, because this is the compartment that has been shown to be associated with a clear biologic consequence: silencing of the associated gene [47]. Using Student's *t* test we found thirty-two gene promoter CpG islands that displayed statistically significant different frequencies of hypermethylation between AR^+ and AR^- xenografts (Figure 5A; $P < 0.01$). Of these, pyrosequencing analysis confirmed the differential methylation of 4 of 5 randomly chosen gene promoter CpG islands: CNN3, GAS6, SOX8, and MAP6 (Figure 5B). Two of these 4 (CNN3 and GAS6) were also found to be differentially methylated by pyrosequencing in a small set

of DNA samples obtained from 5 AR^+ and 4 AR^- patients' tumor samples that were unrelated to the xenografts (Figure 5B).

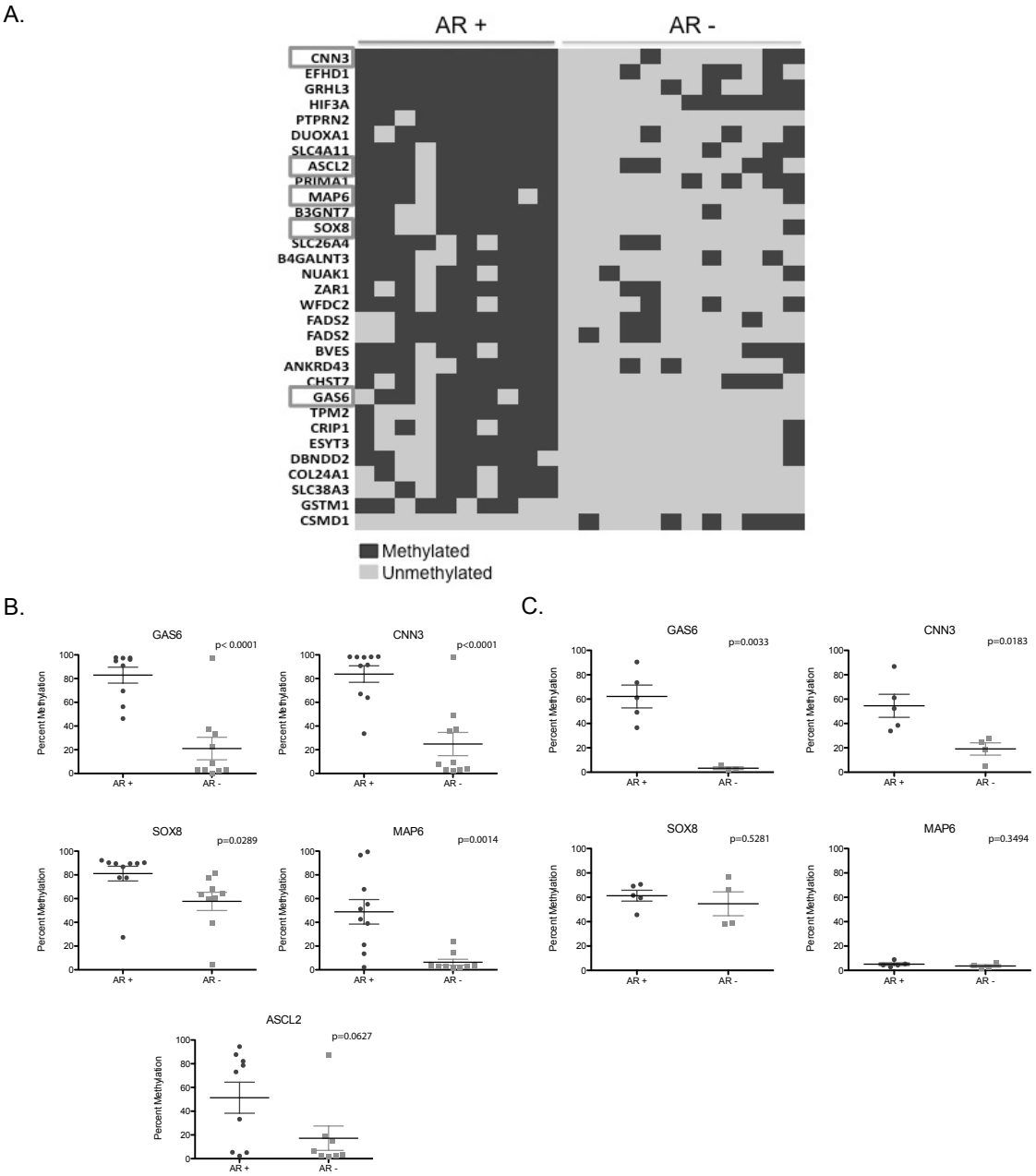

Figure 5. DNA Methylation Markers A. Gene promoter CpG islands differentially methylated between AR^+ and AR^- xenografts. B. Validation by pyrosequencing in DNA extracted from xenograft tumors. C. Validation by pyrosequencing in DNA extracted from 9 unrelated patient tumors.

Differential DNA Methylation Markers Between AR$^-$SCPC and AR$^+$ADENO Xenografts

To determine whether DNA methylation markers distinguished AR$^-$SCPC from AR$^+$ADENO we excluded samples with ADENO morphology that did not express AR (MDA 40, MDA-51, MDA 62, MDA 66, MDA 94 and MDA 118b), the xenograft with squamous cell morphology (MDA 100), the xenografts for which morphology was unknown (MDA-102 and MDA-46) and the "misclassified" MDA 144-20 and MDA 144-11 sublines. This left 9 AR$^-$SCPC and 3 AR$^-$LCNEC (previously found to be biologically similar to AR-SCPC [21]) xenograft samples (n=12) plus 1 mixed AR$^-$SCPC and AR$^+$ADENO derived from 5 patient donor tumors and 10 AR$^+$ADENO xenograft samples derived from 10 patient donor tumors. Unsupervised hierarchical clustering using the top 10 percent hypervariable probes of the 14,821 SmaI sites (as described above) from the averaged probe M values per patient converted to categorical values (log2R/G≥1.3 = methylated, log2R/G<1.3 = unmethylated) showed separate clusters (with the exception of two xenografts, 79 and 101) that distinguishes the AR$^-$SCPC and AR$^+$ADENO morphological groups (Figure 6). Additionally, a Student's t test was performed to determine candidate genes that stratify these groups. There were 250 genes with a p-value<0.01. From these, we chose 10 genes based on gene function and validation with data gathered in the Illumina Infinium Methylation 450k Beadchips (see data below). These genes will be used for future validation on patient samples (*RCCD1, IGF2BP1, TMPRSS2, LPHN1, HAND2, KCNV1, PDE1C, PROKR2, KIRREL, HOXD4*).

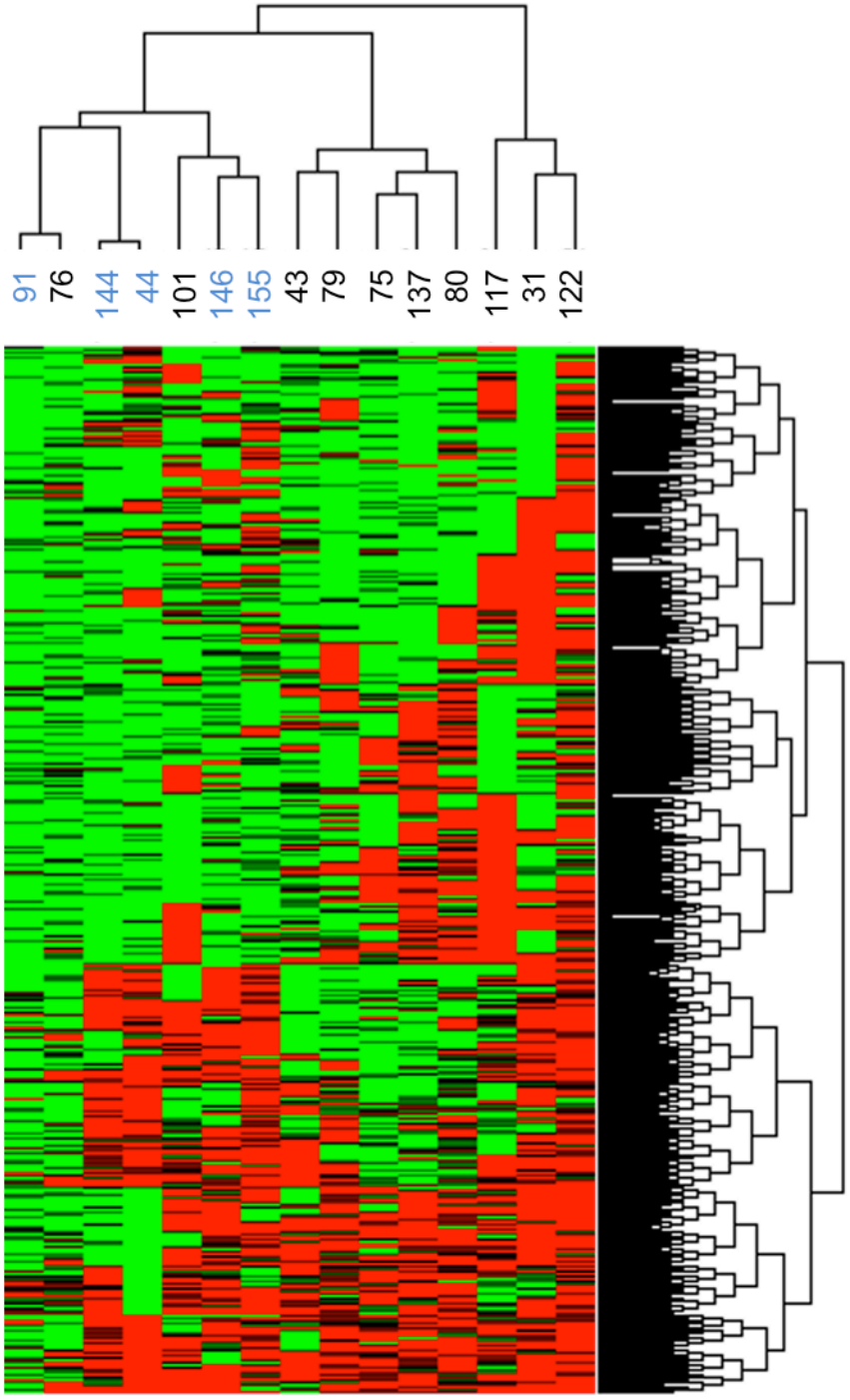

Figure 6. Differential DNA Methylation Markers Between AR^- SCPC and AR^+ ADENO Xenografts. Unsupervised hierarchical clustering using the top 10% hypervariable probes of the averaged probe M values per patient converted to categorical values (log2R/G≥1.3 = methylated, log2R/G<1.3 = unmethylated).

Xenografts Reflect Patient Donor Methylation Patterns

To compare global methylation of primary patient tissues to matched xenograft tissues and the stability of the methylome after tumor passage from human to mouse, we employed the Illumina Infinium Methylation 450k Beadchips (Illumina, San Diego, CA) platform. Patient donor tumor DNA was available for xenografts MDA 144-4, MDA 146-10, MDA 150-10, MDA 153-14, MDA 170-1 and MDA 180-14. DNA from MDA 144-4 and MDA 146-10 were analyzed by MCAM as above (Table 1). Xenografts MDA 170-1 and MDA 180-14 have been described previously [20]. The Infinium methylation array provides comprehensive coverage of the gene including six areas around the CpG island—north shelf (flanking upstream of shore), north shore (flanking upstream of island), island, south shore (flanking downstream of island), south shelf (flanking downstream of shore), and no island. These areas are in relation to known UCSC CpG islands and cover gene regions with sites in the promoter region, 5'UTR, first exon, gene body, and 3'UTR. We evaluated the frequency of methylation changes, referring to a significant methylation increase as 20% greater than the primary sample and significant methylation decrease as 20% greater than the primary sample, between the xenografts and matched patient samples within these regions (Figure 7A). We observed a higher frequency in hypomethylation among the xenograft samples as compared to their patient donor with the highest in the 180-30 (Figure 7B). Overall, frequencies of significant methylation changes, for the most part, were below 10%, therefore,

we feel the xenografts retain the methylation patterns to that of their patient primary sample.

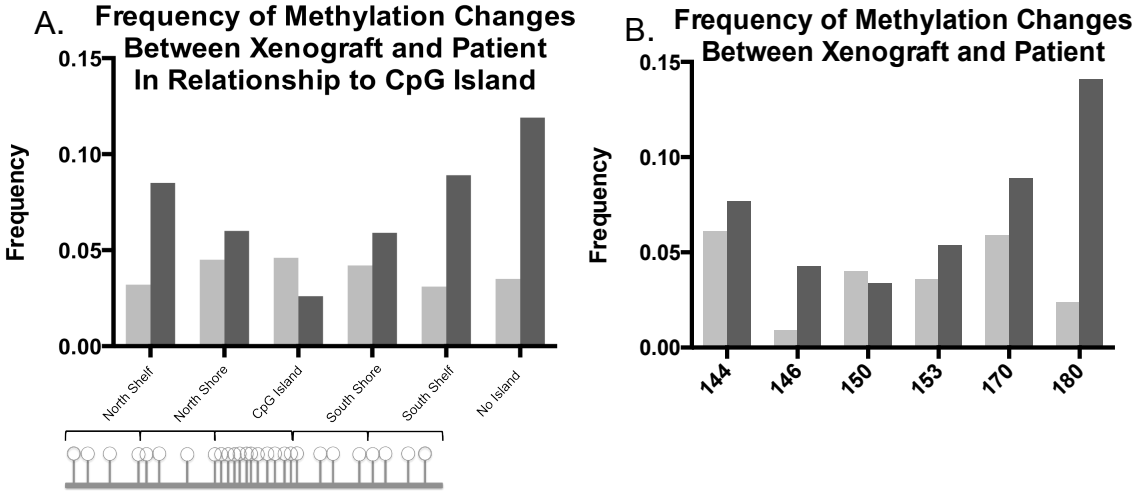

Figure 7. Frequency of Methylation Changes Between Xenograft and Patient. The frequency of methylation changes between xenograft and primary patient samples using the Illumina Infinium Methylation 450k Beadchips. A. The frequency represents the average percentage of probes with 20% more methylation in the xenograft than the patient (light grey bars) and the average percentage of probes among all patients with 20% less methylation in the xenograft than the patient (dark grey bars) broken down by island regions. The schematic below the graph depicts the location of the regions as compared to the CpG island (lollipop figures represent CpG sites). B. The frequency of methylation changes by patient. The light grey bars represent the frequency of methylation increases by 20%, while the dark grey bars represent the frequency of methylation decreases by 20%.

AR Promoter Methylation Is Rare in CRPC

A large CpG island spans the promoter and exon 1 of the androgen receptor gene and previous reports have shown DNA hypermethylation in this region resulting in AR gene silencing in prostate cancer cells. [48, 49] Our previous work had shown that both the AR protein and mRNA transcripts were absent in our AR^-SCPC models and array CGH experiments did not reveal AR deletions.[20] We were struck by the low levels of methylation observed in the

AR promoter of the AR$^-$SCPC xenografts. Therefore, we examined the methylation of the AR promoter-associated CpG island using bisulfite pyrosequening (Figure 8A) in DNA extracted from 11 AR$^+$ and 19 AR$^-$ patient derived xenografts, a xenograft derived cell line [144.13c], as well as the prostate cancer cell lines LNCaP, PC3, NCI H660 and DU145. Of the cell lines, only PC3 and DU145, have more than 15% methylation, confirming what others have reported [31]. All but 4 of the xenografts had less than 15% methylation at the AR promoter regardless of AR expression status (Figure 8B). Our results indicate DNA methylation of the AR promoter is infrequent in CRPC.

A.

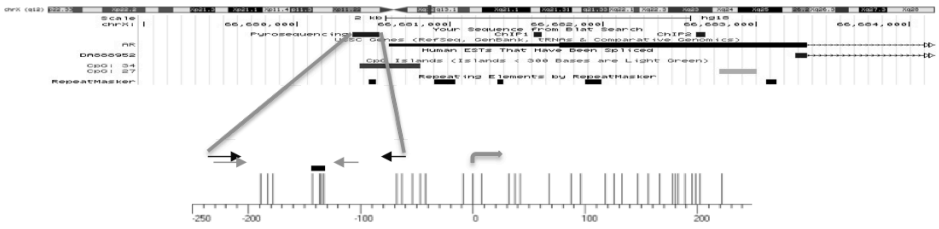

B.

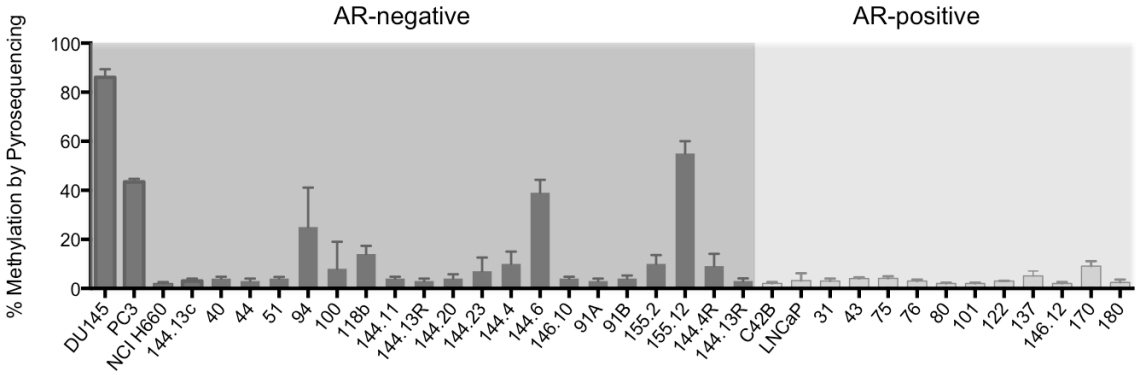

Figure 8. AR Promoter DNA Methylation (A) Pyrosequencing Primer Location. The top bar indicates the chromosomal location of the AR gene. Directly below shows the AR promoter region including the location of the pyrosequencing primers (indicated by a black bar labeled Pyrosequencing) and the CpG island. A more detailed schematic of the pyrosequencing primers are displayed with black arrows (the first step PCR primers), grey arrows (the second step PCR primers), and the black bar (the selected CpG sites). The vertical lines are individual CpG sites with and angled grey arrow above representing the transcription start site (ATG). ChIP-PCR primers are represented by 2 black bars labeled ChIP1 and ChIP2. (B) AR promoter methylation by bisulfite pyrosequencing in AR-negative (black) and AR-positive (grey) prostate cancer xenografts.

H3K27me3 is Enriched at the AR promoter in AR-SCPC Xenografts

We then examined the chromatin markings on the AR promoter using ChIP-qPCR in the previously described AR^-SCPC/LCNEC (MDA PCa 144.13, MDA PCa 144.4, MDA PCa 155.2 and MDA PCa 146.10) and AR^+ADENO (MDA PCa 170.4 and MDA PCa 180.30) xenografts [20, 21]) as well as in three established prostate cancer cell lines (one AR-positive [LNCaP] and two AR-negative [PC3 and DU145]). We evaluated both active, H3K4me3 and H3K9ac, and repressive H3K9me2 and H3K27me3 histone modifications using the marking of the constitutively expressed gene Actinβ (ACTB) and a repressed gene in prostate tissue, Human β-globin (HBB), as controls for these experiments. As expected, the only samples with AR marking by H3K4me3 and/or H3K9ac were the two AR-positive xenografts MDA PCa 170.4 and MDA PCa 180.30 and LNCaP. Marking by repressive histone modifications was more variable: H3K27me3 was a universal finding in AR-negative samples, and was accompanied by H3K9me2 in two out of four xenografts (Figure 9).

It is important to note that DU145 and PC3 both have marked enrichment of H3K27me3 and H3K9me2 along with high promoter methylation. Previous reports have shown that there is a strong correlation between H3K9me2 and DNA methylation. In contrast, H3K27me3 based silencing is independent of DNA methylation and some genes in the PC3 cell line are targeted by both silencing mechanisms, but this seems to be a rare observation. [50] Consequently, we focused on H3K27me3 as the possible mechanism for AR silencing in SCPC.

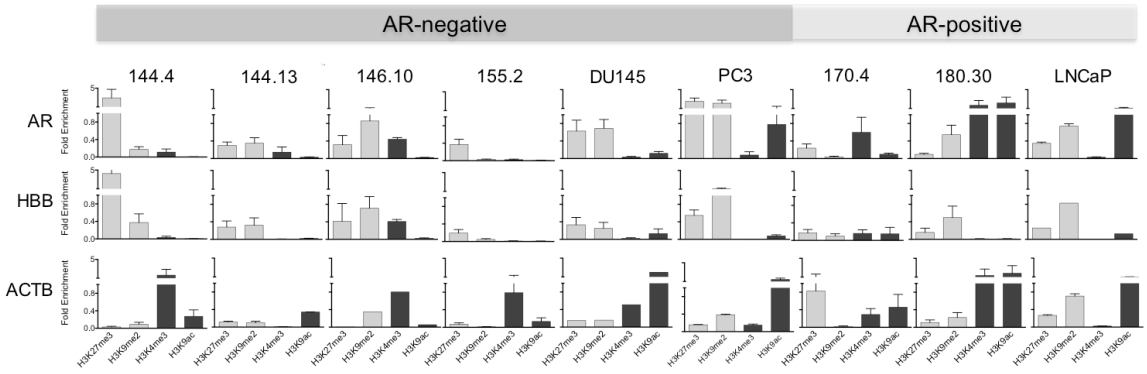

Figure 9. AR Promoter Histone Modifications. Results of ChIP-PCR experiments for repressive marks (H3K27me3 and H3K9me2) in grey and active histone marks (H3K4me3 and H3K9ac) in black at the AR promoter region in AR- SCPC xenografts (144.4, 144.13, 146.10 and 155.2) and AR- cell lines (DU145 and PC3) and AR+ CRPC xenografts (170.4 and 180.30) and cell line LNCaP. HBB and ACTB were used as repressive and active mark controls respectively. The y-axis indicates fold enrichment compared to total histone H3 using the ΔCT method.

Global EZH2 and H3K27me3 levels did not appear different between AR$^-$SCPC and AR$^+$ADENO models

H3K27me3 gene silencing involves polycomb group protein EZH2 which correlates with the aggressiveness of prostate cancer and is known to be overexpressed in multiple cancers [38]. We therefore looked at the global protein expression of H3K27me3 and EZH2 in our xenograft samples and cell lines. Using western blot analysis, we observed similar levels of global protein expression of both H3K27me3 and EZH2 in the AR$^-$ xenografts and cell lines as compared to the AR$^+$ xenograft (Figure 10).

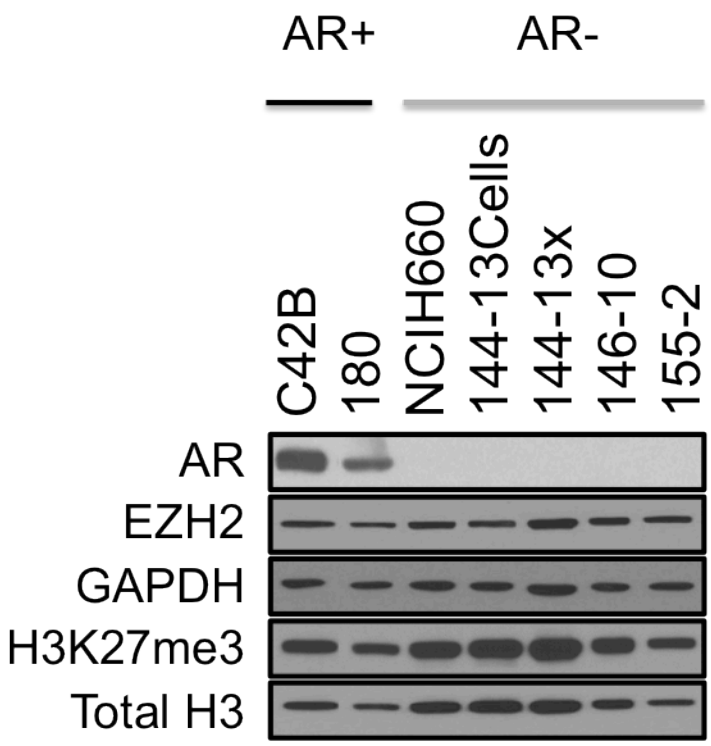

Figure 10. Global levels of EZH2 and H3K27me3. Western blot analysis showing levels of AR, EZH2 and H3K27me3 in and AR^+ CRPC cell line C42B and xenografts (180) and AR^- SCPC cell line NCI H660 and xenografts (144-13, 146-10, 155-2). Control genes GAPDH and total H3 were used for loading.

DZNep treatment induces AR expression in AR-SCPC cell lines

To confirm H3K27me3 based silencing of the AR promoter in SCPC, we evaluated whether inhibition of EZH2 methyltransferase activity could result in AR reexpression. We used DZNep, a known S-adenosylhomocysteine (AdoHcy) hydrolase inhibitor, which leads to the indirect inhibition of methyltransferase activity by blocking S-adenosyl-methionine (AdoMet) dependent reactions. [44] Previous reports have shown a correlation between a decrease in H3K27me3 by DZNep treatment and an increase of gene expression. [44] We treated two AR-

SCPC cell lines, NCI H660 and 144.13, with 0.1, 1 and 5 uM DZNep for 72 hours and evaluated AR expression following treatment by qPCR (Figure 11A). We observed a trend toward increase AR mRNA expression in both 144-13 and NCI H660 cell lines with 1 and 5 uM DZnep treatment. Although we did not see a statistically significant increase in AR transcript levels following treatment, we tested whether the slight increase resulted in protein translation. Using western blot analysis we evaluated the expression of AR with DZNep treatment (Figure 11B). In both NCI H660 and 144-13 cells AR was reexpressed after only 0.1 uM of the drug. The protein appears to increase with drug concentration in both cell lines. However, we see more protein expression in the 144-13 cell line than the NCI H660 cells in contrast to what we observed at the mRNA level where there was more mRNA expression in the NCI H660 cells. Additionally we examined the effect of DZNep on global EZH2 and H3K27me3 in these cells. There was no effect on EZH2 levels at 0.1 and 1 μM DZNep, whereas 5 μM DZNep caused a slight reduction similar to previous reports at 5 μM [51]. However, we did detect a significant reduction in H3K27me3 with treatment, also similar to previous studies. [44, 45] Finally, we observed a dose dependent growth inhibition in both cell lines (Figure 11C).

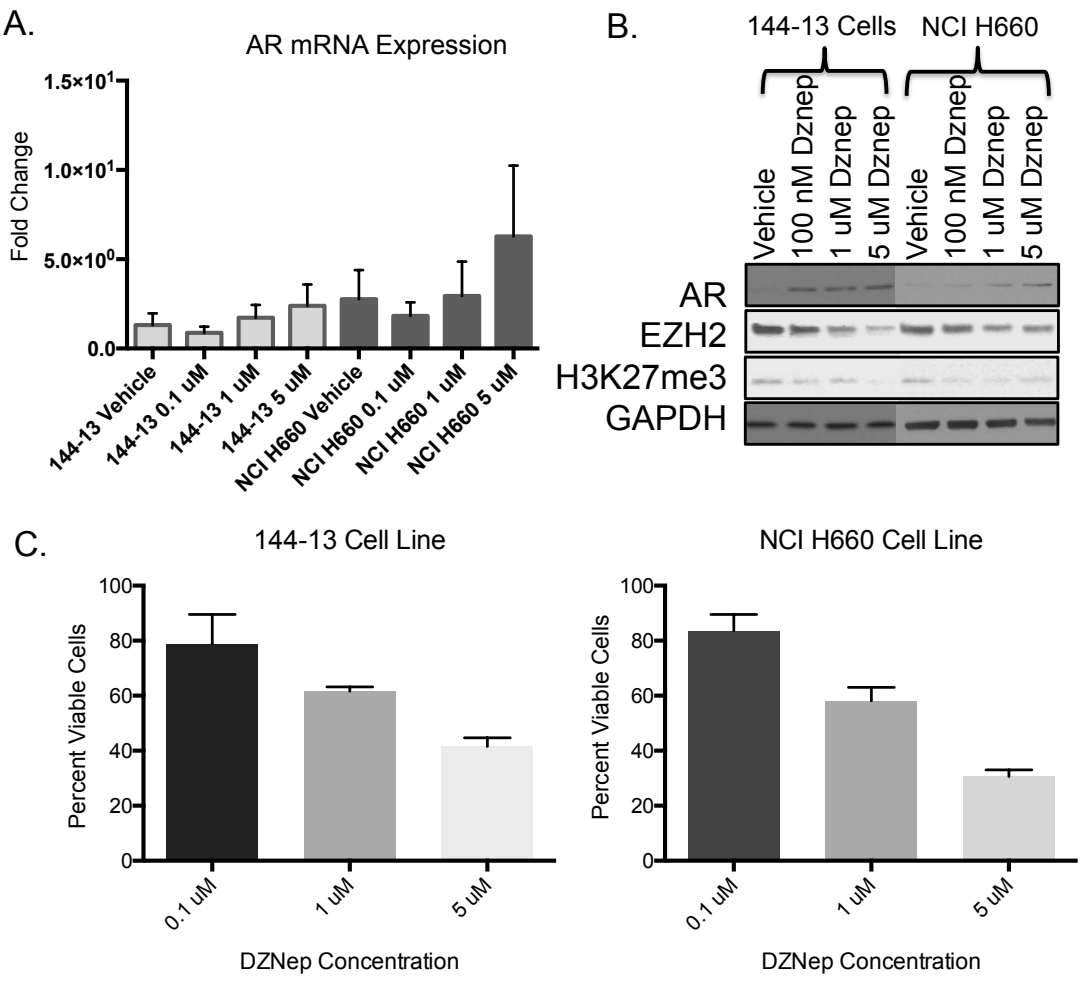

Figure 11. DZNep treatment induces AR expression in AR-SCPC cell lines. A. Quantitative RT-PCR showing AR mRNA expression following 72 hour DZNep treatment in 144-13 and NCIH660 cell lines. Fold change was calculated using the 2^ddCT method to matched untreated cell lines. B. Western blot analysis of the AR, EZH2, and H3K27me3 protein following 72 hour DZNep treatment in 144-13 and NCIH660 cell lines. GAPDH was used as a loading control. C. Percent of viable cells after 72 hours of DZNep treatment as compared to vehicle treated.

Materials and Methods

Tissues and Cells

The prostate cancer cell lines (DU145, LNCaP, PC-3, and NCI-H660) were obtained from the American Type Culture Collection (ATCC) and cultured according to their recommendations. The xenografts samples were provided by the Prostate Cancer Xenograft Bank at The University of Texas MD Anderson

Cancer Center. Donor patient features are located in Table 2 and previously described [20]. 144-13 xenograft derived cell line was developed at MD Anderson Cancer Center. Description of this cell line will be available in a future publication. All cell lines were tested and certified.

DNA Extraction

The DNA was obtained via standard proteinase K and phenol–chloroform extraction technique and quantified on a NanoDrop 1000 spectrophotometer (Thermo Fisher Scientific, Waltham, MA, USA).

DNA was extracted from FFPE patient samples by using the Cold Spring Harbor protocol [52]. Briefly, xylene (cat. no. X5P-1GAL, Fisher Chemical, Fairlawn, NJ, USA) was used for deparaffinization followed by protease digestion and DNA isolation using a RecoverAll total nucleic acid isolation kit (cat. no. AM1975, Ambion Life Technologies Corp., Carlsbad, CA, USA).

Quantitative PCR of Mouse and Human β Globins

Quantitative PCR (qPCR) was performed on genomic DNA from each xenograft sample in 20-µl reactions using iTaq Supermix with ROX (Bio-Rad Laboratories, Hercules, CA) and TaqMan primers and probes specific for the human and mouse βglobin genes designed with Primer Express software (Applied Biosystems Life Technologies, Grand Island, NY). All probes were labeled with the 6-carboxyfluorescein fluorophore (6-FAM) and a custom-synthesized nonfluorescent MGB quencher from Applied Biosystems. Primer and

probe sequences are (a) murine βglobin assay, Mu-bglo-239F, 5'-AGGCCCATGGCAAGAAAGT-3', Mu-bglo-306R, 5'-GCCCTTGAGGCTGTCCAA-3', and Mu-bglo-259T (MGB probe, FAM labeled), 5'-ATAACTGCCTTTAACGATG-3' and (b) human βglobin assay, hu-bglo-232F, 5'-TGAAGGCTCATGGCAAGAAA-3', hu-bglo-285R, 5'-GGTGAGCCAGGCCATCAC-3', and hu-bglo-253T (MGB probe, FAM labeled), 5'-TGCTCGGTGCCTTT-3'. The primers were used at 900 nM and the probes at 100 nM concentrations.

Known quantities of human and mouse DNA was used to construct a standard curve for both primer sets to determine the efficiency of each qPCR. Using the specific mouse βglobin gene, we determined cycle at threshold (Ct) values for each sample and a control containing 100% mouse DNA and their differences, delta Ct (ΔCt), using the Stratagene Mx3005P system (Agilent Technologies, Inc., Santa Clara, CA). Relative amounts of mouse DNA contamination were calculated (by using $2^{-\Delta Ct}$) and then converted to the overall percentage of mouse DNA found in each sample.

MCAM Analysis

A pool of genomic DNA extracted from normal male human peripheral blood mononuclear cells (PBMC) was used as a control for methylated CGI amplification (MCA) and coupled to CGI microarray as previously described [46, 53]. Briefly, following digestion with SmaI and XmaI (New England BioLabs, Inc., Ipswich, MA), DNA was ligated to RMCA PCR adapters and amplified. Amplicons

from xenograft samples were labeled with Cy5 dye and cohybridized against amplicons from PBMC labeled with Cy3 dye on Agilent Technologies 4 ´ 44K custom DNA microarrays. The 42,222 probes (corresponding to 8,321 unique RefSeq genes) on the array recognize SmaI/XmaI fragments predominantly located around gene transcription start sites (TSSs). Fluorescence signals were LOWESS normalized, [54] and trimmed averages of normalized log2 ratios were calculated for amplicons covered by multiple probes. Hypermethylation was defined as normalized log2 ratio of Cy5/Cy3 fluorescence (M values) greater than 1.3 (equivalent to 2.5-fold and higher of xenografts/control signal intensity) on the basis of prior experimental data [46].

Pyrosequencing

Validation of the methylation status of candidate genes was performed using bisulfite Pyrosequencing methylation analysis. Briefly, 1.5 μg of genomic DNA was subjected to bisulfite treatment with an EpiTect bisulfite kit (Qiagen). The bisulfite-treated DNA (40 ng) was amplified in a two-step PCR. A 20-μl reaction was carried out for each gene in 67 mmol/l Tris-HCl (pH 8.8), 16 mmol/l ammonium sulfate, 2 mmol/l $MgCl_2$, 0.125 mmol/l dNTPs, 1 unit of Taq polymerase, and 100 nmol/l PCR primers (Table 4). TQ21 oligonucleotide (10 nmol/l) was used as a reversible inhibitor of Taq polymerase in the first step of the PCR [55]. The second step of the PCR was used to label one DNA strand with biotin by using a universal primer tag, excluding LINE-1, which was biotinylated, at the 5′ end [56]. The second reaction contained all of the elements

just described plus 4.5 pmol of biotinylated universal primer (5′-biotin-GGGACACCGCTGATCGTTTA-3′), 1 ml of PCR product from the first step, and new forward and reverse primers in which the reverse primer contained a 20-bp linker sequence (Table 3). PCR cycling conditions were 30 seconds at 95 °C, 30 seconds at the respective annealing temperature, and 30 seconds at 72 °C for 40 cycles. The biotinylated PCR product was bound to Streptavidin-Sepharose HP (GE Healthcare, Piscataway, NJ, USA), made single stranded, and purified to act as a template in the Pyrosequencing reaction as recommended by the manufacturer by using the Pyrosequencing Vacuum Prep Tool (Qiagen). Then, 0.3-μM gene-specific Pyrosequencing primer was annealed to the purified single-stranded PCR product, and Pyrosequencing was performed by using the PSQ HS 96 Pyrosequencing System (Qiagen). The raw data was analyzed using the allele quantitation algorithm on the Pyro Q-CpG software (Qiagen). The percentage methylation of each gene was computed as the average of two to four CpG sites.

Table 3. Pyrosequencing Primers

Gene		Primer Sequence 5' to 3'	Annealing Temperature	Distance From Studied CpGs to SmaI Site	Distance of the SmaI Site to Gene TSS
ASCL2	F1	ATTGGGAATGGGGGTGGAT			
	R1	ATACCCCCCAAAACCCTCA	58	0	-477
	S	AGTATTTTGTTTGTGGTT			
ASCL2	F1	GGGTGGTTTAAGATTGGTTGAGA			
	R1	CAAAAACCCCCAAACCTT	58	-9	-86
	S	TTTTAGGTTTTAGGAGGG			
FOXI2	F1	GGGAGGGGAGGAAAATTGAT			
	R1	CACTAACCACCCATCCAACTTAA	60	-24	-518
	S	TTTATGGGTTTTGGTTT			
FOXI2	F1	GGAGAGGTTGGATATGGTTATTT			
	R1	CTAACCCCTTCACCCACAAA	58	65	-83
	S	GGTTGGATATGGTTATTTAT			
HAND 1	F1	AGGAAAAGGGGGAGTGGTTA	60	-56	-23
	R1	CCCATTCCCAATCCCTACTAAC			

	S	GAGTGGTTATTTTAGGTTTT			
HAND 1	F1	GGGGGAGGGGATAAGGAAAA			
	R1	CCCATTCCCAATCCCTACTAAC	60	-56	-23
	S	GAGTGGTTATTTTAGGTTTT			
SOX3	F1	GGTGAAAAGGTTTTGGGATTT			
	R1	CCCCCCAATTCCTACTAATTTAA	58	-66	172
	S	GGGGTTTGTGGGTTA			
SOX3	F1	GGAATTGGTAGTTGGTTGTTTAGA			
	R1	CAAACCCCCAAAAACCTCAC	56	11	-673
	R2	AAAACCTATCTCCCATACCC			
	S	TTTTTTTAGGAGGGTTAGT			
SOX 9	F1	AGAGGAGAAGGTATTAAAATTTTG			
	R1	AAAAAATCCCAACCAAAAAA	60	101	362
	S	AATTTATATATTTGGAAGTT			
NEUROD2	F1	GTATGAGTTTGTATTGGGGGAGA			
	R1	AAAAAACAACTCCTCCCACCTTC	56	0	-119
	S	TTTGTATTGGGGGAGA			
POU4F2	F1	GTATTGGGTTGGGAGTTTAGAGT			
	R1	CCACCACCCCTAAAAACACA	60	-128	-1479
	S	GGGTTGGGAGTTTAGAG			
CNN3	F1	GAGGTGAGGGAAGAAGTAGG			
	R1	CCTCCTCCCCAACTCTAAACCC	58	45	-333
	S	TTGTTATTGGTGTTTTAGTAG			
MAP6	F1	GAGGGATTTTATAGATTTTTTTAGGATAGT			
	R1	ACCTCCTCTTTCTTCTTATAATTCTA	60	0	-98
	S	ATAGATTTTTTTAGGATAGTTTTT			
SOX8	F1	TGGATTATTTATGGGGAGGGAGT			
	R1	ACTCCTACCCTCCCTACTT	58	-118	888
	S	TATGGGGAGGGAGTG			
GAS6	F1	TTGTTTTTAGGAGAGTATTTGGTAG			
	R1	ACCCTCCCTCTACTAAACTAA	60	0	851
	R2	AAAAATAAAAAACAATCCCCTCC			
	S	AGGAGAGTATTTGGTAGAA			
AR	F1	TAGGAAGTAGGGGTTTTTTAGGGTTAG			
	R1	ACCCAACCCACCTCCTTACCT			
	F2	GTAGGGGTTTTTTAGGGTTAGAGTTAGT	56/60	-115	9
	R2	GGGACACCGCTGATCGTTTA			
	S	TTGTTTTTTTAAAGTTATTAGGTA			
BMP6	F1	TTAGGGGAGTTTTTAGTTGTTTAG			
	R1	CCTCCAAACCATTCTCCTAATA	60	257	-240
	S	GTTTAGGTTAGAGAGGTGG			
NEP	F1	GGGATTTGTTGAGGGGTTA			
	R1	AACACCTAAACATCCCTCC	60		
	S	GATTTGTTGAGGGGTTA			
CAV1	F1	TGGTTGTTTATATTGGGTATT			
	R1	AAACAACATTTTCCCTACTCT			
	S	GTTTATATTGGGTATTTTTGTA	56	-49	-76
GSTP1	F1	GGGAGTTAGAGGGATTTTTTAGAAGA			
	R1	CCACCTCCCAACCTTATAAAAATAAT			
	R2	CCCTCCCCCCCAATACTAAATCA			
	S	GAGGGATTTTTTAGAAGAG	60	-111	80
RARb	F1	ATTTTTTGTTAAAGGGGGGATTAGA			
	R1	CCATACCCAAACAAACCCTACTC			
	S	TTTGAGGATTGGGATG	60		
RASSF1	F1	ATGTAGGGGGAGTTTGAGTTTATTGA			
	R1	CACCACCCCCCAAATAAAATC	60	-1670	-234

	F2	GTTGGGAGAGTTGGGAAGGGT			
	R2	ACACCACCCCCCAAATAAAATC			
	S	AGGGTYGTATTYGGTTGGA			
SLC16A12	F1	GGTTTAGGTGATAAGGGTATTTTTTAAGG			
	R1	TAGAGGGAGAGGTGGTTTAGGTGAT			
	R2	CACCCAAATTAAAATCCCAAACTC			
	S	AAGGGTATTTTTTAAGGAAG	58	147	-5
LINE1	F1	TTTTTTGAGTTAGGTGTGGG			
	R1	biotin-TCTCACTAAAAAATACCAAACAA			
	S	GGGTGGGAGTGA	54		

Illumina Infinium Methylation 450k Beadchips

DNA was extracted as described above from FFPE patient donor tumors and matched xenograft tissues. Genomic DNA from MDA 144-4, MDA 146-10, MDA 150-10, MDA 153-14, MDA 170-1 and MDA 180-14 xenograft and donor patient samples were run on a 0.8% agarose gel to determine the quality of the sample. Genome-wide methylation analysis was performed by the University of Southern California Epigenome Center, Los Angeles, CA on the Illumina Infinium Methylation 450k array.

Chromatin Immunoprecipitation

Fresh xenograft tissues were enzymatically dissociated using 10 mL of Accumax - Cell Aggregate Dissociation Medium (eBioscience, 00-4666-56) per gram of tissue, were incubated at 37 for 30 minutes under constant agitation. The cells were strained, washed with PBS and counted for crosslinking. ChIP assays were performed by treating the cells in culture and the xenograft cells with 1% formaldehyde to cross-link histones to DNA. The crosslinking was stopped by 0.125 M glycine for 5 minutes and then washed with cold PBS containing

protease inhibitor cocktail (Roche). The chromatin was then extracted, fragmented by sonication, and the lystate was immunoprecipitated using Dynal Protein G magnetic beads and the following antibodies: H3K4me3 (Millipore, 17-614), H3K9ac (Millipore, 07-352), H3K9me2 (Abcam, ab1220), H3K27me3 (Millipore, 17-622), histone H3 (Abcam, ab1791-100), and rabbit IgG (Abcam, ab46540). ChIP products were used for TaqMan quantitative PCR with oligonucleotide primers covering two regions of the AR exon 1, and positive controls of active Actinβ and repressed genes HBB. The fold enrichment of each histone modification to histone H3 was calculated using the ΔCt method.

Cell Culture and Drug Treatment

NCI-H660 and 144-13 cells were grown in RPMI-1640 with 5% FBS, 100 ug/ml penicillin/streptomycin solution. Cells were seeded 300,000 per 10-cm dish 72 hours prior to treatment. Cells were then treated with 0.1, 1, and 5 umol/L DZNep for 72 hrs. The cells were harvested and counted using the Vi-CELL Series Cell Viability Analyzer (Beckman Coulter).

Western Blotting

Protein extracts for were prepared by homogenizing the tissues and cells in lysis buffer supplemented with Complete Protease (Roche). Soluble proteins were separated by SDS-PAGE, and transferred to PVDF membranes (BIO-RAD). Membranes were incubated with mouse anti-EZH2 (3827-1, Epitomics), rabbit anti-H3K27me3 (9733s, Cell Signaling), rabbit anti-GAPDH (2118s, Cell

Signaling), rabbit anti-AR (n-20, Santa Cruz) and rabbit anti-histone H3 (Abcam, ab1791-100). The antigen-antibody complexes were detected by Luminata Western HRP substrate (Millipore).

qPCR

Total RNA (1 ug) was extracted using TRI-reagent (Invitrogen) followed by Direct-zol RNA MiniPrep Kit (Zymo) according to the manufacturer's instructions. The first-strand cDNA was synthesized using the High-Capacity cDNA Reverse Transcription (Life Technologies, Inc.). Quantitative PCR (qPCR) was performed with the Universal PCR Master Mix (Applied Biosystems) and AR Taqman probe/primer (Hs00171172_m1, Life Technologies) using ABI Prism 7500. Results were obtained from 3 independent experiments in triplicate with Actin Beta (Hs99999903_m1, Life Technologies) as the reference gene. Fold change was calculated using 2^delta delta CT method.

Chart review

The electronic medical records of the 24 patients from whose tumors the xenografts were obtained were retrospectively reviewed under MD Anderson's IRB-approved protocol RCR06-1075 to extract the patients' relevant clinicopathologic features.

Discussion

This study delves into the epigenetics of CRPC in an effort to understand the biology of the disease, determine clinically relevant biomarkers that classify CRPC into subgroups and seek possible therapeutic targets. We show that DNA methylation profiling of CRPC xenograft tumors supports the widely accepted notion that CRPCs are heterogeneous. Our goal was to use DNA methylation as a tool to develop noninvasive biomarkers that can guide treatment decisions for patients with CRPC. Aberrantly hypermethylated DNA sequences can be detected in the peripheral circulation; therefore, differentially methylated DNA sequences could stratify clinically relevant tumor subtype [57, 58]. We compared the DNA methylation profiles of AR^{+}ADNEO *vs*. AR^{-}SCPC xenografts because although the AR is now known to be a central driver of a large proportion of CRPCs, a subset of CRPCs adopt SCPC morphological features, lose AR expression, and are associated with a clinically distinct and aggressive course despite a unique responsiveness to chemotherapy [4, 8, 59].

Although we did identify a small subset of methylated genes that distinguish AR^{-}SCPC from AR^{+}ADENO CRPC tissues, we did not find a methylated sequence that might identify the emergence of SCPC/AR^{-} variants. Additionally these markers will need further validation using matched donor patient samples. These distinguishing methylated genes may only represent the heterogeneity of the disease and not the underlying biology of the SCPC phenotype.

Our finding that the DNA methylation profiles of xenograft sublines derived from a single donor patient's tumor, but grown in different mice, were more similar to each other than they were to the profiles of tumors derived from different patients suggesting that DNA methylation profiles are stable in xenografts and likely reflect those of patient's tumors. This is further supported by our validation in patient samples of the different methylation of the GAS6 and CNN3 promoters, although not all genes were validated because available patient samples, while representative of the AR^{+}ADNEO and AR^{-}SCPC disease, they were not matched to the xenografts studied and the numbers were small. Moreover, approximately 20% of our CRPC tumors were characterized by lower levels of methylation at promoter CpG islands, similar to previous studies using patient tumor samples [34]. Additional studies with larger numbers of related donor patients' tumor samples will be necessary to confirm that the DNA methylation profiles of CRPC xenografts accurately reflect the methylation profiles in the donor patients' tumors.

It must be noted that our DNA methylation profiling method identifies *SmaI/XmaI* fragments predominantly located in CpG islands around gene TSSs. Some authors contend that tissue- and cancer-specific differently methylated regions are located predominantly at DNA methylation shores, regions of low CpG density located near traditional CpG islands [60]. It is possible that the use of genome-wide methylation analysis with techniques such as bisulfite conversion combined with next-generation sequencing (BS-seq) will successfully identify differently methylated regions among the CRPC subsets.

Furthermore, immunohistochemical studies have shown that in most prostate cancer tissues (both untreated and castrate resistant), AR staining is heterogeneous, [61, 62] and that increased heterogeneity in AR expression is more frequent in less-differentiated prostate cancers [63]. Our observations and those of Friedlander *et al*. and Hill *et al*. raise the question of whether an epigenetic modifier is deregulated in the subset of tumors characterized by lower levels of methylation [34, 64]. Recent studies have shown that epigenetic modifiers are often mutated in cancers including prostate cancer [10]. The histone methyltransferase, *MLL2*, specific for H3K4 methylation, is mutated in 6% of CRPC along with an 8% rate of mutation or deletion in *CHD1*, which encodes an ATP-dependent chromatin-remodeling enzyme [10]. Furthermore, studies have shown increased levels of DNA methyltransferase 1 (DNMT1) protein and of DNMT3A2, DNMT3B, and EZH2 transcripts in untreated primary prostate tumors, relative to the levels in benign prostate tissues.

It is clear that the androgen receptor plays a central role in prostate cancer and its progression. While AR is oncogenic in prostate cancer and its inhibition produces therapeutic responses, the loss of AR expression is associated with dedifferentiation of prostate cancer and an aggressive clinical behavior. Therefore, it is important to determine the underlying mechanism that contributes to it loss of expression. Epigenetic gene silencing has been implicated in multiple cancers, including prostate cancer, most notably DNA methylation [44]. We examined the promoter associated CpG island of the AR gene and determined, while there are some samples containing DNA methylation, AR silencing is not a

result of DNA methylation in CRPC. Therefore we explored an alternate epigenetic pathway responsible for gene silencing and most often independent of DNA methylation, the polycomb repressor complex 2 which has been implicated in the progression of prostate cancer including the overexpression of EZH2 [35, 38, 50, 65]. We did not detect overexpression of EZH2 in the AR^-SCPC as compared to the AR^+ADENO. Aberrant EZH2 activity is not limited to overexpression, but could reflect a change in activity of ncRNA binding to PRC2 and regulating the maintenance of a repressed state [66]. PRC2 has a higher affinity for longer ncRNAs and thus an increase in lncRNAs that recruit PRC2 to the chromatin could account for the increased H3K27me3 at the AR locus without an increase in EZH2 protein [42, 66]. Nonetheless, we demonstrate that the AR gene promoter is enriched in H3K27me3 histone marks and its subsequent removal with DZNep results in AR mRNA and protein re-expression. While we have shown one mechanism responsible for AR silencing in AR^-SCPC, it is difficult to determine, at this point, if the re-expression of AR contributes to the cell death we observed *in vitro*. DZNep was an important tool to assist us in establishing a functional relationship between EZH2, H3K27me3, and AR expression in SCPC, however its selectivity for EZH2 is poor and was found to globally inhibit both repressive and active histone methylation marks [44]. Recently, a highly selective, small-molecule inhibitor of EZH2 methyltransferase activity was developed by GlaxoSmith Klein, GSK126.[67] GSK126 decreases global H3K27me3 levels and reactivates silenced PRC2 target genes by competitively inhibiting the methyltransferase S-adenosyl-methionine (SAM) [67].

Interestingly, EZH2 could be a transcriptional coactivator of AR instead of the transcriptional repressor of PCR2, as it is thought to be in CRPC, through phosphatidylinositol 3-kinase–Akt (PI3K) pathway mediating the phosphorylation of EZH2 at Ser21 [65]. These investigators, however, used AR^+ CRPC cell lines that do not represent the AR^-SCPC we are studying. Therefore, while the EZH2 function of coactivation could play a role in AR^-SCPC, our data supports its repressor function at the AR locus. More studies are necessary to fully understand the epigenomic functional role in of EZH2 in AR^-SCPC.

SCPC represents a small subset of CRPC, bearing distinguishable morphological, clinical, genetic and epigenetic features that reflect an undifferentiated cellular program. Here we challenge the accepted role that AR activation stimulates proliferation and propose its reactivation in SCPC could result in tumor suppressive effects. Our findings reflect the complexity and diversity of epigenetic regulation in prostate cancer and underscore the importance for developing pharmacologic approaches for effective epigenetic gene reactivation.

REFERENCES

1. Taylor, B.S., N. Schultz, H. Hieronymus, A. Gopalan, Y. Xiao, B.S. Carver, V.K. Arora, P. Kaushik, E. Cerami, B. Reva, Y. Antipin, N. Mitsiades, T. Landers, I. Dolgalev, J.E. Major, M. Wilson, N.D. Socci, A.E. Lash, A. Heguy, J.A. Eastham, H.I. Scher, V.E. Reuter, P.T. Scardino, C. Sander, C.L. Sawyers, and W.L. Gerald, *Integrative genomic profiling of human prostate cancer.* Cancer Cell, 2010. **18**(1): p. 11-22.
2. Gleason, D.F., *Classification of prostatic carcinomas.* Cancer Chemother Rep, 1966. **50**(3): p. 125-8.
3. Logothetis, C.J., G.E. Gallick, S.N. Maity, J. Kim, A. Aparicio, E. Efstathiou, and S.H. Lin, *Molecular classification of prostate cancer progression: foundation for marker-driven treatment of prostate cancer.* Cancer Discov, 2013. **3**(8): p. 849-61.
4. Ryan, C.J., M.R. Smith, J.S. de Bono, A. Molina, C.J. Logothetis, P. de Souza, K. Fizazi, P. Mainwaring, J.M. Piulats, S. Ng, J. Carles, P.F. Mulders, E. Basch, E.J. Small, F. Saad, D. Schrijvers, H. Van Poppel, S.D. Mukherjee, H. Suttmann, W.R. Gerritsen, T.W. Flaig, D.J. George, E.Y. Yu, E. Efstathiou, A. Pantuck, E. Winquist, C.S. Higano, M.E. Taplin, Y. Park, T. Kheoh, T. Griffin, H.I. Scher, D.E. Rathkopf, and C.-A.-. Investigators, *Abiraterone in metastatic prostate cancer without previous chemotherapy.* N Engl J Med, 2013. **368**(2): p. 138-48.

5. Scher, H.I., K. Fizazi, F. Saad, M.E. Taplin, C.N. Sternberg, K. Miller, R. de Wit, P. Mulders, K.N. Chi, N.D. Shore, A.J. Armstrong, T.W. Flaig, A. Flechon, P. Mainwaring, M. Fleming, J.D. Hainsworth, M. Hirmand, B. Selby, L. Seely, J.S. de Bono, and A. Investigators, *Increased survival with enzalutamide in prostate cancer after chemotherapy.* N Engl J Med, 2012. **367**(13): p. 1187-97.

6. Moore, S.R., Y. Reinberg, and G. Zhang, *Small cell carcinoma of prostate: effectiveness of hormonal versus chemotherapy.* Urology, 1992. **39**(5): p. 411-6.

7. Tanaka, M., Y. Suzuki, K. Takaoka, N. Suzuki, S. Murakami, O. Matsuzaki, and J. Shimazaki, *Progression of prostate cancer to neuroendocrine cell tumor.* Int J Urol, 2001. **8**(8): p. 431-6; discussion 437.

8. Papandreou, C.N., D.D. Daliani, P.F. Thall, S.M. Tu, X. Wang, A. Reyes, P. Troncoso, and C.J. Logothetis, *Results of a phase II study with doxorubicin, etoposide, and cisplatin in patients with fully characterized small-cell carcinoma of the prostate.* J Clin Oncol, 2002. **20**(14): p. 3072-80.

9. Lotan, T.L., B. Gurel, S. Sutcliffe, D. Esopi, W. Liu, J. Xu, J.L. Hicks, B.H. Park, E. Humphreys, A.W. Partin, M. Han, G.J. Netto, W.B. Isaacs, and A.M. De Marzo, *PTEN protein loss by immunostaining: analytic validation and prognostic indicator for a high risk surgical cohort of prostate cancer patients.* Clin Cancer Res, 2011. **17**(20): p. 6563-73.

10. Grasso, C.S., Y.M. Wu, D.R. Robinson, X. Cao, S.M. Dhanasekaran, A.P. Khan, M.J. Quist, X. Jing, R.J. Lonigro, J.C. Brenner, I.A. Asangani, B. Ateeq, S.Y. Chun, J. Siddiqui, L. Sam, M. Anstett, R. Mehra, J.R. Prensner, N. Palanisamy, G.A. Ryslik, F. Vandin, B.J. Raphael, L.P. Kunju, D.R. Rhodes, K.J. Pienta, A.M. Chinnaiyan, and S.A. Tomlins, *The mutational landscape of lethal castration-resistant prostate cancer.* Nature, 2012. **487**(7406): p. 239-43.

11. Aparicio, A., R.B. Den, and K.E. Knudsen, *Time to stratify? The retinoblastoma protein in castrate-resistant prostate cancer.* Nat Rev Urol, 2011. **8**(10): p. 562-8.

12. Yu, J., J. Yu, R.S. Mani, Q. Cao, C.J. Brenner, X. Cao, X. Wang, L. Wu, J. Li, M. Hu, Y. Gong, H. Cheng, B. Laxman, A. Vellaichamy, S. Shankar, Y. Li, S.M. Dhanasekaran, R. Morey, T. Barrette, R.J. Lonigro, S.A. Tomlins, S. Varambally, Z.S. Qin, and A.M. Chinnaiyan, *An integrated network of androgen receptor, polycomb, and TMPRSS2-ERG gene fusions in prostate cancer progression.* Cancer Cell, 2010. **17**(5): p. 443-54.

13. King, J.C., J. Xu, J. Wongvipat, H. Hieronymus, B.S. Carver, D.H. Leung, B.S. Taylor, C. Sander, R.D. Cardiff, S.S. Couto, W.L. Gerald, and C.L. Sawyers, *Cooperativity of TMPRSS2-ERG with PI3-kinase pathway activation in prostate oncogenesis.* Nat Genet, 2009. **41**(5): p. 524-6.

14. Hoogland, A.M., G. Jenster, W.M. van Weerden, J. Trapman, T. van der Kwast, M.J. Roobol, F.H. Schroder, M.F. Wildhagen, and G.J. van Leenders, *ERG immunohistochemistry is not predictive for PSA*

recurrence, local recurrence or overall survival after radical prostatectomy for prostate cancer. Mod Pathol, 2012. **25**(3): p. 471-9.

15. Fine, S.W., A. Gopalan, M.A. Leversha, H.A. Al-Ahmadie, S.K. Tickoo, Q. Zhou, J.M. Satagopan, P.T. Scardino, W.L. Gerald, and V.E. Reuter, *TMPRSS2-ERG gene fusion is associated with low Gleason scores and not with high-grade morphological features.* Mod Pathol, 2010. **23**(10): p. 1325-33.
16. Verras, M., J. Lee, H. Xue, T.H. Li, Y. Wang, and Z. Sun, *The androgen receptor negatively regulates the expression of c-Met: implications for a novel mechanism of prostate cancer progression.* Cancer Res, 2007. **67**(3): p. 967-75.
17. Varkaris, A., A.D. Katsiampoura, J.C. Araujo, G.E. Gallick, and P.G. Corn, *Src signaling pathways in prostate cancer.* Cancer Metastasis Rev, 2014.
18. Liu, Y., M. Karaca, Z. Zhang, D. Gioeli, H.S. Earp, and Y.E. Whang, *Dasatinib inhibits site-specific tyrosine phosphorylation of androgen receptor by Ack1 and Src kinases.* Oncogene, 2010. **29**(22): p. 3208-16.
19. Ro, J.Y., B. Tetu, A.G. Ayala, and N.G. Ordonez, *Small cell carcinoma of the prostate. II. Immunohistochemical and electron microscopic studies of 18 cases.* Cancer, 1987. **59**(5): p. 977-82.
20. Tzelepi, V., J. Zhang, J.F. Lu, B. Kleb, G. Wu, X. Wan, A. Hoang, E. Efstathiou, K. Sircar, N.M. Navone, P. Troncoso, S. Liang, C.J. Logothetis, S.N. Maity, and A.M. Aparicio, *Modeling a lethal prostate cancer variant*

with small-cell carcinoma features. Clin Cancer Res, 2012. **18**(3): p. 666-77.

21. Aparicio, A., V. Tzelepi, J.C. Araujo, C.C. Guo, S. Liang, P. Troncoso, C.J. Logothetis, N.M. Navone, and S.N. Maity, *Neuroendocrine prostate cancer xenografts with large-cell and small-cell features derived from a single patient's tumor: morphological, immunohistochemical, and gene expression profiles.* Prostate, 2011. **71**(8): p. 846-56.
22. Mosquera, J.M., H. Beltran, K. Park, T.Y. MacDonald, B.D. Robinson, S.T. Tagawa, S. Perner, T.A. Bismar, A. Erbersdobler, R. Dhir, J.B. Nelson, D.M. Nanus, and M.A. Rubin, *Concurrent AURKA and MYCN gene amplifications are harbingers of lethal treatment-related neuroendocrine prostate cancer.* Neoplasia, 2013. **15**(1): p. 1-10.
23. Guo, C.C., J.Y. Dancer, Y. Wang, A. Aparicio, N.M. Navone, P. Troncoso, and B.A. Czerniak, *TMPRSS2-ERG gene fusion in small cell carcinoma of the prostate.* Hum Pathol, 2011. **42**(1): p. 11-7.
24. Beltran, H., D.S. Rickman, K. Park, S.S. Chae, A. Sboner, T.Y. MacDonald, Y. Wang, K.L. Sheikh, S. Terry, S.T. Tagawa, R. Dhir, J.B. Nelson, A. de la Taille, Y. Allory, M.B. Gerstein, S. Perner, K.J. Pienta, A.M. Chinnaiyan, Y. Wang, C.C. Collins, M.E. Gleave, F. Demichelis, D.M. Nanus, and M.A. Rubin, *Molecular characterization of neuroendocrine prostate cancer and identification of new drug targets.* Cancer Discov, 2011. **1**(6): p. 487-95.

25. Clegg, N., C. Ferguson, L.D. True, H. Arnold, A. Moorman, J.E. Quinn, R.L. Vessella, and P.S. Nelson, *Molecular characterization of prostatic small-cell neuroendocrine carcinoma.* Prostate, 2003. **55**(1): p. 55-64.

26. Lapuk, A.V., C. Wu, A.W. Wyatt, A. McPherson, B.J. McConeghy, S. Brahmbhatt, F. Mo, A. Zoubeidi, S. Anderson, R.H. Bell, A. Haegert, R. Shukin, Y. Wang, L. Fazli, A. Hurtado-Coll, E.C. Jones, F. Hach, F. Hormozdiari, I. Hajirasouliha, P.C. Boutros, R.G. Bristow, Y. Zhao, M.A. Marra, A. Fanjul, C.A. Maher, A.M. Chinnaiyan, M.A. Rubin, H. Beltran, S.C. Sahinalp, M.E. Gleave, S.V. Volik, and C.C. Collins, *From sequence to molecular pathology, and a mechanism driving the neuroendocrine phenotype in prostate cancer.* J Pathol, 2012. **227**(3): p. 286-97.

27. Westermark, U.K., M. Wilhelm, A. Frenzel, and M.A. Henriksson, *The MYCN oncogene and differentiation in neuroblastoma.* Semin Cancer Biol, 2011. **21**(4): p. 256-66.

28. Aparicio, A., C.J. Logothetis, and S.N. Maity, *Understanding the lethal variant of prostate cancer: power of examining extremes.* Cancer Discov, 2011. **1**(6): p. 466-8.

29. Lister, R., M. Pelizzola, R.H. Dowen, R.D. Hawkins, G. Hon, J. Tonti-Filippini, J.R. Nery, L. Lee, Z. Ye, Q.M. Ngo, L. Edsall, J. Antosiewicz-Bourget, R. Stewart, V. Ruotti, A.H. Millar, J.A. Thomson, B. Ren, and J.R. Ecker, *Human DNA methylomes at base resolution show widespread epigenomic differences.* Nature, 2009. **462**(7271): p. 315-22.

30. Jones, P.A. and S.B. Baylin, *The epigenomics of cancer.* Cell, 2007. **128**(4): p. 683-92.

31. Yegnasubramanian, S., J. Kowalski, M.L. Gonzalgo, M. Zahurak, S. Piantadosi, P.C. Walsh, G.S. Bova, A.M. De Marzo, W.B. Isaacs, and W.G. Nelson, *Hypermethylation of CpG islands in primary and metastatic human prostate cancer.* Cancer Res, 2004. **64**(6): p. 1975-86.

32. Yang, A.S., M.R. Estecio, K. Doshi, Y. Kondo, E.H. Tajara, and J.P. Issa, *A simple method for estimating global DNA methylation using bisulfite PCR of repetitive DNA elements.* Nucleic Acids Res, 2004. **32**(3): p. e38.

33. Aryee, M.J., W. Liu, J.C. Engelmann, P. Nuhn, M. Gurel, M.C. Haffner, D. Esopi, R.A. Irizarry, R.H. Getzenberg, W.G. Nelson, J. Luo, J. Xu, W.B. Isaacs, G.S. Bova, and S. Yegnasubramanian, *DNA methylation alterations exhibit intraindividual stability and interindividual heterogeneity in prostate cancer metastases.* Sci Transl Med, 2013. **5**(169): p. 169ra10.

34. Friedlander, T.W. and C.J. Ryan, *Targeting the androgen receptor.* Urol Clin North Am, 2012. **39**(4): p. 453-64.

35. Cao, R., L. Wang, H. Wang, L. Xia, H. Erdjument-Bromage, P. Tempst, R.S. Jones, and Y. Zhang, *Role of histone H3 lysine 27 methylation in Polycomb-group silencing.* Science, 2002. **298**(5595): p. 1039-43.

36. Chase, A. and N.C. Cross, *Aberrations of EZH2 in cancer.* Clin Cancer Res, 2011. **17**(9): p. 2613-8.

37. Arisan, S., E.D. Buyuktuncer, N. Palavan-Unsal, T. Caskurlu, O.O. Cakir, and E. Ergenekon, *Increased expression of EZH2, a polycomb group protein, in bladder carcinoma.* Urol Int, 2005. **75**(3): p. 252-7.

38. Varambally, S., S.M. Dhanasekaran, M. Zhou, T.R. Barrette, C. Kumar-Sinha, M.G. Sanda, D. Ghosh, K.J. Pienta, R.G. Sewalt, A.P. Otte, M.A. Rubin, and A.M. Chinnaiyan, *The polycomb group protein EZH2 is involved in progression of prostate cancer.* Nature, 2002. **419**(6907): p. 624-9.

39. Watanabe, H., K. Soejima, H. Yasuda, I. Kawada, I. Nakachi, S. Yoda, K. Naoki, and A. Ishizaka, *Deregulation of histone lysine methyltransferases contributes to oncogenic transformation of human bronchoepithelial cells.* Cancer Cell Int, 2008. **8**: p. 15.

40. Zeidler, M., S. Varambally, Q. Cao, A.M. Chinnaiyan, D.O. Ferguson, S.D. Merajver, and C.G. Kleer, *The Polycomb group protein EZH2 impairs DNA repair in breast epithelial cells.* Neoplasia, 2005. **7**(11): p. 1011-9.

41. Varambally, S., Q. Cao, R.S. Mani, S. Shankar, X. Wang, B. Ateeq, B. Laxman, X. Cao, X. Jing, K. Ramnarayanan, J.C. Brenner, J. Yu, J.H. Kim, B. Han, P. Tan, C. Kumar-Sinha, R.J. Lonigro, N. Palanisamy, C.A. Maher, and A.M. Chinnaiyan, *Genomic loss of microRNA-101 leads to overexpression of histone methyltransferase EZH2 in cancer.* Science, 2008. **322**(5908): p. 1695-9.

42. Cheng, W., Z. Zhang, and J. Wang, *Long noncoding RNAs: new players in prostate cancer.* Cancer Lett, 2013. **339**(1): p. 8-14.

43. Kotake, Y., T. Nakagawa, K. Kitagawa, S. Suzuki, N. Liu, M. Kitagawa, and Y. Xiong, *Long non-coding RNA ANRIL is required for the PRC2 recruitment to and silencing of p15(INK4B) tumor suppressor gene.* Oncogene, 2011. **30**(16): p. 1956-62.

44. Miranda, T.B., C.C. Cortez, C.B. Yoo, G. Liang, M. Abe, T.K. Kelly, V.E. Marquez, and P.A. Jones, *DZNep is a global histone methylation inhibitor that reactivates developmental genes not silenced by DNA methylation.* Mol Cancer Ther, 2009. **8**(6): p. 1579-88.

45. Tan, J., X. Yang, L. Zhuang, X. Jiang, W. Chen, P.L. Lee, R.K. Karuturi, P.B. Tan, E.T. Liu, and Q. Yu, *Pharmacologic disruption of Polycomb-repressive complex 2-mediated gene repression selectively induces apoptosis in cancer cells.* Genes Dev, 2007. **21**(9): p. 1050-63.

46. Estecio, M.R., P.S. Yan, A.E. Ibrahim, C.S. Tellez, L. Shen, T.H. Huang, and J.P. Issa, *High-throughput methylation profiling by MCA coupled to CpG island microarray.* Genome Res, 2007. **17**(10): p. 1529-36.

47. Baylin, S.B. and P.A. Jones, *A decade of exploring the cancer epigenome - biological and translational implications.* Nat Rev Cancer, 2011. **11**(10): p. 726-34.

48. Jarrard, D.F., H. Kinoshita, Y. Shi, C. Sandefur, D. Hoff, L.F. Meisner, C. Chang, J.G. Herman, W.B. Isaacs, and N. Nassif, *Methylation of the androgen receptor promoter CpG island is associated with loss of androgen receptor expression in prostate cancer cells.* Cancer Res, 1998. **58**(23): p. 5310-4.

49. Jarrard, D.F., *More data on locally extensive prostate cancer--betting on the margin.* J Urol, 2000. **163**(4): p. 1189-90.

50. Kondo, Y., L. Shen, A.S. Cheng, S. Ahmed, Y. Boumber, C. Charo, T. Yamochi, T. Urano, K. Furukawa, B. Kwabi-Addo, D.L. Gold, Y. Sekido, T.H. Huang, and J.P. Issa, *Gene silencing in cancer by histone H3 lysine 27 trimethylation independent of promoter DNA methylation.* Nat Genet, 2008. **40**(6): p. 741-50.

51. Sato, T., A. Kaneda, S. Tsuji, T. Isagawa, S. Yamamoto, T. Fujita, R. Yamanaka, Y. Tanaka, T. Nukiwa, V.E. Marquez, Y. Ishikawa, M. Ichinose, and H. Aburatani, *PRC2 overexpression and PRC2-target gene repression relating to poorer prognosis in small cell lung cancer.* Sci Rep, 2013. **3**: p. 1911.

52. Tang, W., F.B. David, M.M. Wilson, B.G. Barwick, B.R. Leyland-Jones, and M.M. Bouzyk, *DNA extraction from formalin-fixed, paraffin-embedded tissue.* Cold Spring Harb Protoc, 2009. **2009**(2): p. pdb prot5138.

53. Toyota, M., C. Ho, N. Ahuja, K.W. Jair, Q. Li, M. Ohe-Toyota, S.B. Baylin, and J.P. Issa, *Identification of differentially methylated sequences in colorectal cancer by methylated CpG island amplification.* Cancer Res, 1999. **59**(10): p. 2307-12.

54. Yang, M.C., Q.G. Ruan, J.J. Yang, S. Eckenrode, S. Wu, R.A. McIndoe, and J.X. She, *A statistical method for flagging weak spots improves normalization and ratio estimates in microarrays.* Physiol Genomics, 2001. **7**(1): p. 45-53.

55. Yakimovich, O.Y., Y.I. Alekseev, A.V. Maksimenko, O.L. Voronina, and V.G. Lunin, *Influence of DNA aptamer structure on the specificity of binding to Taq DNA polymerase.* Biochemistry (Mosc), 2003. **68**(2): p. 228-35.

56. Colella, S., L. Shen, K.A. Baggerly, J.P. Issa, and R. Krahe, *Sensitive and quantitative universal Pyrosequencing methylation analysis of CpG sites.* Biotechniques, 2003. **35**(1): p. 146-50.

57. Aparicio, A., B. North, L. Barske, X. Wang, V. Bollati, D. Weisenberger, C. Yoo, N. Tannir, E. Horne, S. Groshen, P. Jones, A. Yang, and J.P. Issa, *LINE-1 methylation in plasma DNA as a biomarker of activity of DNA methylation inhibitors in patients with solid tumors.* Epigenetics, 2009. **4**(3): p. 176-84.

58. Kwee, S., M.A. Song, I. Cheng, L. Loo, and M. Tiirikainen, *Measurement of circulating cell-free DNA in relation to 18F-fluorocholine PET/CT imaging in chemotherapy-treated advanced prostate cancer.* Clin Transl Sci, 2012. **5**(1): p. 65-70.

59. Spiess, P.E., C.A. Pettaway, F. Vakar-Lopez, W. Kassouf, X. Wang, J.E. Busby, K.A. Do, R. Davuluri, and N.M. Tannir, *Treatment outcomes of small cell carcinoma of the prostate: a single-center study.* Cancer, 2007. **110**(8): p. 1729-37.

60. Irizarry, R.A., C. Ladd-Acosta, B. Wen, Z. Wu, C. Montano, P. Onyango, H. Cui, K. Gabo, M. Rongione, M. Webster, H. Ji, J.B. Potash, S. Sabunciyan, and A.P. Feinberg, *The human colon cancer methylome*

shows similar hypo- and hypermethylation at conserved tissue-specific CpG island shores. Nat Genet, 2009. **41**(2): p. 178-86.

61. van der Kwast, T.H., J. Schalken, J.A. Ruizeveld de Winter, C.C. van Vroonhoven, E. Mulder, W. Boersma, and J. Trapman, *Androgen receptors in endocrine-therapy-resistant human prostate cancer.* Int J Cancer, 1991. **48**(2): p. 189-93.

62. Hobisch, A., Z. Culig, C. Radmayr, G. Bartsch, H. Klocker, and A. Hittmair, *Distant metastases from prostatic carcinoma express androgen receptor protein.* Cancer Res, 1995. **55**(14): p. 3068-72.

63. Magi-Galluzzi, C., X. Xu, L. Hlatky, P. Hahnfeldt, I. Kaplan, P. Hsiao, C. Chang, and M. Loda, *Heterogeneity of androgen receptor content in advanced prostate cancer.* Mod Pathol, 1997. **10**(8): p. 839-45.

64. Hill, V.K., C. Ricketts, I. Bieche, S. Vacher, D. Gentle, C. Lewis, E.R. Maher, and F. Latif, *Genome-wide DNA methylation profiling of CpG islands in breast cancer identifies novel genes associated with tumorigenicity.* Cancer Res, 2011. **71**(8): p. 2988-99.

65. Xu, K., Z.J. Wu, A.C. Groner, H.H. He, C. Cai, R.T. Lis, X. Wu, E.C. Stack, M. Loda, T. Liu, H. Xu, L. Cato, J.E. Thornton, R.I. Gregory, C. Morrissey, R.L. Vessella, R. Montironi, C. Magi-Galluzzi, P.W. Kantoff, S.P. Balk, X.S. Liu, and M. Brown, *EZH2 oncogenic activity in castration-resistant prostate cancer cells is Polycomb-independent.* Science, 2012. **338**(6113): p. 1465-9.

66. Davidovich, C., L. Zheng, K.J. Goodrich, and T.R. Cech, *Promiscuous RNA binding by Polycomb repressive complex 2.* Nat Struct Mol Biol, 2013. **20**(11): p. 1250-7.

67. McCabe, M.T., H.M. Ott, G. Ganji, S. Korenchuk, C. Thompson, G.S. Van Aller, Y. Liu, A.P. Graves, A. Della Pietra, 3rd, E. Diaz, L.V. LaFrance, M. Mellinger, C. Duquenne, X. Tian, R.G. Kruger, C.F. McHugh, M. Brandt, W.H. Miller, D. Dhanak, S.K. Verma, P.J. Tummino, and C.L. Creasy, *EZH2 inhibition as a therapeutic strategy for lymphoma with EZH2-activating mutations.* Nature, 2012. **492**(7427): p. 108-12.

VITA

Brittany North Kleb was born in Garland, Texas on January 24, 1981. She attended Southern Methodist University and received her Bachelor of Science Degree in Biology in 2003. She began working at The University of Texas MD Anderson Cancer Center in 2007 and enrolled in the Master of Science program in Biomedical Sciences at the Graduate School of Biomedical Sciences in 2011 under the direction of Dr. Ana Aparicio.